SOIL STORAGE ON STEEP FORESTED AND NON-FORESTED MOUNTAIN HILLSLOPES IN THE BITTERROOT MOUNTAINS, MONTANA

by

Colin Aidan Quinn

A thesis submitted in partial fulfillment
of the requirements for the degree

of

Master of Science

in

Earth Sciences

MONTANA STATE UNIVERSITY
Bozeman, Montana

May 2018

ACKNOWLEDGEMENTS

I would like to acknowledge the people and resources that allowed for the completion of this thesis. Firstly, the project would not have been possible without the help of Dr. Jean Dixon for guiding me from an archaeological background into the world of hillslope geomorphology. From new lab techniques to providing endless rounds of edits and even hauling logs off snowy forest service roads, I was able to rely on Jean's experience at every step along the way. I would also like to acknowledge my committee of Dr. Dave McWethy and Dr. Stephanie Ewing for input on project creation, its findings, and patience with the process. The Bitterroot and Sapphire Mountains project would not be as extensive as it is without previous foundational work from Sarah Benjaram and collaboration at the University of Montana with Dr. Andrew Wilcox.

Every project also requires funding and space to make it successful. To this end, I thank the generosity of NSF-GLD1644624, NSF-EPS110142, the MSU Institute on Ecosystems, the Donald L. Smith Memorial Fund, and LiDAR imagery provided by an NSF NCALM seed grant to Sarah Benjaram. Thank you to LeaAnne Harbour for lab assistance at MSU's Gamma Spectroscopy Lab and to the MSU Earth Surface Processes Lab Group (Grace Nicholas, Kailey Adams, Erin Shervey, Aaron Feldhaus).

Finally, without support from Singer Horse Capture, my family, and my friends this project would have been a much different endeavor.

TABLE OF CONTENTS

LIST OF TABLES

LIST OF FIGURES

ABSTRACT

Mountain hillslopes are dynamic settings with discontinuous soils affected by a suite of variables including climate, lithology, hydrology, and vegetation. Our study seeks to understand how forest cover influences soil and rock distribution at decadal to century timescales. We focus on a series of post-glacial hillslopes in Lost Horse Creek of the Bitterroot Mountains, Montana. In this system, avalanche paths maintain parallel, topographically similar swaths of forested and non-forested slopes with uniform aspect, lithology, and climate. We combine field observations, fallout radionuclide analysis ($^{210}Pb_{ex}$ & ^{137}Cs), and remote sensing data to understand both landscape- and fine-scale patterns in soil and rock distribution. Local soil and rock measurements indicate more extensive soil cover (forest = 94.4±2.6%; non-forest = 88.3±1.9%) and thicker soils (6cm greater median) in the forested system. We compare landcover-classified rock to topographic metrics from LiDAR data and find a doubling of rock cover (from 40% to 80%) as hillslope angles transition across slopes of ~24-42º. Topographic roughness, calculated as the standard deviation of slope, is predictive of only ~60% of total landscape rock cover, but can identify large boulders and coarse-scale outcrops with higher accuracy (79%). These calibrated remote sensing metrics indicate higher rock cover in non-forested regions (34%, compared to 20% in forested areas), though with high uncertainty. Additionally, we measure fallout-radionuclide inventories in soils to explore variations in decadal transport processes and soil residence times. We find distinct ^{210}Pb and ^{137}Cs behaviors in forested and non-forested systems, controlled both by unique partitioning of each nuclide within organic and mineral soil horizons, but also due to depth-driven differences in their physical mobility. Average $^{210}Pb_{ex}$ inventories in non-forested soils are 33% lower, and half as variable as soils in the forested region (10.45±0.97 and 15.49±1.91 kBq/m^2 respectively), while ^{137}Cs inventories are indistinguishable (4.04±0.34 and 3.73±0.42 kBq/m^2). Together, our spatial, field, and isotope analyses suggest forested systems have greater soil storage and longer residence times than non-forested soils, mediated by differences in surface erosion processes within a larger fire disturbance landscape.

INTRODUCTION

Mountainous landscapes provide a dynamic setting for the interaction of the geosphere, biosphere, and hydrosphere, all of which influence the presence of soils and set the stage for rock and soil weathering and erosion (Dietrich and Perron, 2006; Hahm et al., 2014). Discontinuous soil cover in steep mountain settings results from spatial and temporal differences in denudation (Norton et al., 2014; Milodowski et al., 2015b), but the underlying mechanisms explaining the persistence of soil cover within rapidly eroding systems thought to be bedrock-dominated have been topics of active debate (Dixon and von Blanckenburg, 2012; Heimsath et al., 2012; Larsen et al., 2014; Milodowski et al., 2015a). Understanding soil distribution controls on dynamic, steep hillslopes requires first quantifying soil cover, which itself presents a significant challenge (e.g., Milodowski et al., 2015b). Measuring the magnitude, variation, and patterns of soil and rock cover and their links to topographic variables and erosion rates can provide insight into the mechanisms that control their distribution (Dibiase et al., 2012; Milodowski et al., 2015b).

Soils provide essential substrate and nutrients for vegetation (Amundson et al., 2015; Hahm et al., 2014), and this vegetation in turn strongly influences soil transport on steep hillslopes (Dibiase and Lamb, 2013; Marston, 2010; Milodowski et al., 2015a). Vegetation damming may enable soil storage on steep hillslopes, and presence of plant and associated litter cover can reduce soil erosion by rerouting surface waters, intercepting rain splash, and reducing aeolian transport (Abrahams et al., 1995; Dibiase and Lamb, 2013; Dietrich and Perron, 2006; Miyata et al., 2009; Wainwright et al.,

2000). However, vegetation may also increase soil particle mobilization and transport through root interactions and tree-throw (Gabet, 2003; Roering et al., 2010). This complexity in vegetation-mediated soil transport processes likely plays a vital role in controlling soil distribution in mountainous landscapes at local to landscape scales (Hahm et al., 2014; Milodowski et al., 2015b; Norton et al., 2010). However, limited studies have specifically quantified the influence of vegetation on the spatial and temporal distribution of soil storage on steep hillslopes.

Several methods offer promise for measuring soil cover and erosion. Remotely sensed data (aerial imagery and topography) provide insight into landcover and can be used to quantify the patterns of soil and rock distribution on mountain hillslopes. Topographic variables such as terrain steepness and roughness have previously shown utility in understanding both the distribution and controls on rock and soil cover (Dibiase et al., 2012; Milodowski et al., 2015b). Furthermore, multiple isotope systems are used to track soil erosion processes, enabled by the isotopes' presence within mineral lattices (e.g., in-situ ^{10}Be), or adsorption and binding to the reactive surface of soil particles (e.g., meteoric ^{10}Be and fallout radionuclides such as ^{210}Pb and ^{137}Cs) (Belmont et al., 2014; Dixon and Riebe, 2014; Mabit et al., 2013; Portenga and Bierman, 2011; Rogowski and Tamura, 1970). Applications of these tracers are not without their challenges, and require calibration and testing in rocky mountainous systems, due to heterogeneous soil cover and complex soil transport pathways.

Here, we explore the variation in soil distribution and soil storage at decadal to century timescales in forested and non-forested mountainous hillslopes. Using field

observations, remote sensing landcover classification, and isotopic fallout radionuclide tracers, we first evaluate the efficacy of these methodologies in heterogeneous mountain systems and test and refine their use in assessing soil cover and storage. We use high-resolution aerial imagery to identify landscape-scale rock, soil, and vegetation cover, and test against topographic variables that may be diagnostic of rock exposure in mountainous systems (Dibiase et al., 2012; Milodowski et al., 2015b). Field data is used to ground-truth remote observations, and also measure the variability in rock and soil cover at a local-scale (1m). Analysis of fallout radionuclides in soils then provide a method to assess the relative variability in decadal-to-century scale soil erosion. Together, these methods offer a unique view into the spatial and temporal variability of soil storage on steep mountain landscapes. Comparing data across adjacent, topographically-similar hillslopes, we test if vegetation (forest and non-forest cover) has a measurable influence on soil storage in steep mountain settings.

APPROACH AND METHODS

Field Site

We designed our study to quantify if and how forest cover influences the magnitude and variability of soil storage over decadal to century time scales. Our work focuses on a set of south facing slopes in Lost Horse Creek, within the Bitterroot Mountains of southwest Montana (Figure 1). These slopes are scoured by modern and historic avalanche paths that control vegetation patterns. We focus on a set of hillslopes colloquially referred to as the "Ohio Slide" in Lost Horse Creek (Figure 1), this name referencing the historic avalanche activity, not earthen mass moving events (Stauffer, 1976). These avalanche paths provide unique hillslope settings historically devoid of forested vegetation, and are predominantly covered by beargrass (*Xerophyllum tenax*) and the rare immature alpine larch above 1676m (*Larix lyallii*; Arno and Habeck, 1972; Stauffer, 1976). Avalanche slopes are adjacent to mixed conifer forests of lodgepole pine, subalpine fir, Douglas fir, and large Engelmann spruce (Bernhard, 1899). Controls on timberline are presumed to be climate controlled.

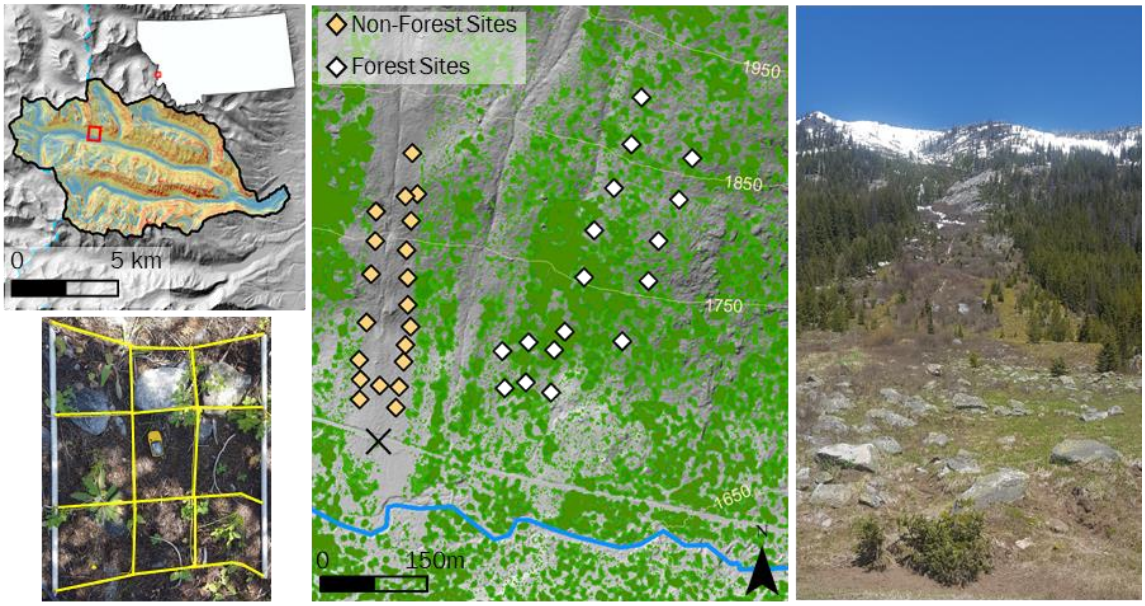

Figure 1: Upper left: The location of Lost Horse Creek watershed, Western Montana displaying slope (red = high slope to blue = low slope). Middle: Sampling locations for forest (white) and non-forest (orange) with LiDAR derived forest canopy height in green (heights > 5m). Lower left: 1m x 1m soil sampling grid. Right: Upslope view of the non-forested 'Ohio Slide' region, photo position indicated by X on middle panel, facing north.

The region of interest is underlain by a lithologically homogenous granitic unit from the Tertiary and Cretaceous Idaho Batholith (Lonn and Berg, 1996). Parallel, east-west trending drainages previously dissected by Pleistocene glaciers flank the eastern side of the mountain range and drain to the Bitterroot River (Alden, 1932). The semi-arid climate is snow dominated, with average annual precipitation of ~1220 mm/yr. Over 60% of precipitation is delivered between November through March, with a persistent snowpack into May and June (PRISM Climate Group).

Previous studies across the Bitterroot Range have exploited the lithologic homogeneity to study effects of glaciation (Naylor and Gabet, 2007), fire impact on sediment yields (Robichaud et al., 2009), and distribution of bedrock exposures

(Milodowski et al., 2015b). Within the Lost Horse catchment, Benjaram (Benjaram, 2017) quantified the variability of soil chemical weathering and used coarse-spatial scale landcover data (30m National Land Cover Database) to understand soil and rock cover. This work highlighted high variability in soil cover and weathering at a landscape scale, and the need for finer scale (1m) analysis. Here, we add to insights from these studies by exploring the patterns and variability of soil storage and rock emergence in the presence of different forested and non-forested vegetation cover.

We use field, geospatial, and isotopic tools to study the variability in soil storage within and between forested and non-forested hillslopes in Lost Horse watershed. We quantify soil cover and thickness at local, 1m scales using field surveys and auger depths to refusal, along with aerial imagery to quantify rock and soil cover at hillslope-scales, and compare this to vegetation and topography (Dibiase et al., 2012; Milodowski et al., 2015b). We then use fallout radionuclides to understand the local and landscape variability in soil residence times and erosion (Appleby and Oldfield, 1978; He and Walling, 1997; Kaste et al., 2006; Rogowski and Tamura, 1970) in the presence or absence of forest cover.

Determining Local Soil Storage

Fallout Radionuclide Analysis

Fallout radionuclides (FRNs) like ^{210}Pb and ^{137}Cs are widely used to understand patterns of sediment transport and storage over decadal to century timescales (e.g., He and Walling, 1997; Kaste et al., 2006). These radioisotopes are produced via geogenic and thermonuclear pathways in the atmosphere, and are deposited on the land surface

adhering rapidly to soil particles (Rogowski and Tamura, 1970). Our analysis focused on two FRNs with unique production and depositional pathways. ^{210}Pb ($t_{1/2}$ = 22.6 years) is a member of the ^{238}U decay series and is found in two forms: in-situ and excess (also referred to as atmospheric or unsupported). Excess ^{210}Pb is derived from atmospheric ^{222}Rn, a daughter of ^{226}Ra, and is continuously deposited on the land surface by precipitation or dust. By contrast, ^{137}Cs ($t_{1/2}$ = 30.17 years) is anthropogenically derived, a byproduct of thermonuclear arms use in the mid-20th century (e.g. Faure and Mensing, 2005). Weapons testing peaked in 1963 which coincides with a peak in ^{137}Cs production and deposition on the Earth's surface (Wright et al., 1999). Upon deposition, $^{210}Pb_{ex}$ and ^{137}Cs bind strongly to soil particles, especially organics and clays (Faure and Mensing, 2005; Lewis, 1977).

Inventories of FRNs within soil profiles are used to assess soil erosion and deposition patterns on hillslopes. Erosion rates can be modeled by identifying 'non-eroding' reference sites, or spatial patterns of inventories on hillslopes can be used to assess relative differences in erosion or deposition (Kaste et al., 2006). The assumptions inherent in these approaches are that FRNs are uniformly delivered across the hillslope and retained in soils, such that spatial heterogeneity in soil inventories reflect erosion processes (Chappell et al., 1998). While local delivery of nuclides via precipitation can be highly differential (Mabit et al., 2013; Parsons and Foster, 2011), landscape delivery variability typically exceeds local variability (Kaste et al., 2006). Importantly, few studies have explored FRN abundances in mountain settings, where variable vegetation and coarse and patchy soil cover add significant complexity to delivery and behavior of FRNs

(Mabit et al., 2013; Parsons and Foster, 2011). In such settings, identification of non-eroding reference sites to calibrate erosion rates is not possible, and assumptions of uniform delivery and chemical retention in surface soil horizons may not be valid (Mabit et al., 2013; Parsons and Foster, 2011).

We focused on two primary aims in fallout radionuclide analysis. Firstly, because studies typically focus on fine soils in non-forested areas for FRN analysis, we needed to assess how FRNs are partitioned in the coarse and sometimes organic-rich soils that we explore here. To do this we measured FRN inventories in separated organic soil and mineral horizons, and also in coarse and fine soil separates. Secondly, we used integrated sampling (1m) to avoid local variability in delivery (Kaste et al., 2006), and a grid-based sampling approach to quantify FRN variability at a hillslope scale in both forested and non-forested regions of our study area (Figure 1). We expected greater FRN inventories in the forested system, communicating longer soil residence times compared to inventories in avalanche impacted non-forested slopes.

Field Data Collection

Field work was carried out in 2016 and 2017 and focused on sampling soils for fallout radionuclide analysis and quantifying the extent of soil cover and thickness at each sample site. Comparison of aerial imagery and LiDAR derived canopy heights showed that a canopy height of >5m over a 3m roving window best corresponded to local continuous forest cover. Within delineated forested and non-forested regions, we mapped out a grid of 42 sites to sample, between 25 and 40m apart. In the field, GPS was used to locate target sites. Only four target sites were deemed inappropriate and not sampled,

including 1 non-forested and 3 forested sites due to the presence of juvenile hardwoods and lack of tree cover, respectively. Forest site grids were shifted east (Figure 1) to avoid a complex drainage upslope of the original sampling grid.

At each of the 38 sites, we used a one-by-one-meter grid segmented into nine, approximately equal sized sections to sample soil and record fine spatial scale (1m) soil distribution. Percent rock cover in each grid was determined by surficial exposure of any lithic object, cobble size or larger (approx. > 64mm). Two types of samples were collected from each grid: a set of surface soil samples and depth of refusal auger samples. At 8 sections of the grid, surface soil samples were collected using a 5cm diameter soil auger to excavate to 20cm, a depth designed to capture the dominant FRN signal (Chappel 1999; Kaste et al., 2007). The eight surface soil samples were combined for analysis to average out local-scale variability in fallout nuclide abundance. In forested samples, the organic litter layer was sampled separately from underlying mineral soil, and the respective thicknesses recorded (e.g., 5cm litter layer + 15cm mineral soil within the 20cm total depth sampled). This design scheme allowed for the collection of organic and mineral soils integrated over a one-by-one-meter grid up to 20cm in depth. An auger core at each site was taken from the grid section of greatest depth, and was sampled in 20cm increments to the depth-of-refusal.

Laboratory Analysis

Auger and soil samples were processed for FRN analysis by first drying field samples at ~80°C for 24 hours. Both organic and mineral horizon samples were sieved into coarse (>2mm) and fine (<2mm) fractions, and were packed separately into 100mm

diameter plastic petri dishes and sealed with electrical tape. All 175 packed samples were set aside for two weeks to establish secular equilibrium for ^{222}Rn (the gaseous parent nuclide of ^{210}Pb; $t_{1/2}$ = 3.8 days). Samples were then analyzed for FRN activities using a Canberra high purity, broad energy germanium detector (BEGe) in the Fallout Radionuclide Laboratory at Montana State University. Nuclide activities in each sample were calculated from measured decays per second using energy and efficiency calibrations based on multi-isotope standards of known activity. The GENIE 2K software was calibrated using these standard activities then energy and efficiency curves were fit to a spectrum to quantify error and accuracy of each nuclide measured. To obtain FRN activities, we took measured counts/sec/kg (CPS/kg) based on count time, sample mass, and kiloelectron volt (keV) level of interest (^{210}Pb is measured at an energy peak of 46 keV, ^{226}Ra at 186 keV, and ^{137}Cs at 661 keV). CPS/kg is divided by the gamma emission probability of the specific FRN and efficiency of the detector to obtain an activity in Becquerels per kilogram (Bq/kg). We determined $^{210}Pb_{ex}$ from total ^{210}Pb counts assuming that $^{210}Pb_{in\text{-}situ}$ is in equilibrium with ^{226}Ra (Faure and Mensing, 2005).

Multiple sample activities were needed to determine total nuclide activity at each $1m^2$ grid site, including the activities of different size fractions for both organic litter and mineral soil layers. The activity of the litter and mineral layers at each grid ($A_{i(T)}$ [Bq/kg]) are separately calculated using particle size component activities and the relative fraction each component contributes to the overall sample mass:

$$A_{i(T)} = \left(A_{i(fine)} * f_{i(fine)}\right) + \left(A_{i(coarse)} * f_{i(coarse)}\right), \qquad \text{(Equation 1)}$$

Here, $f_{i(fine)}$ and $f_{i(coarse)}$ are the relative abundances of fine (>2mm) and coarse (>2mm) soil fractions in a sample from either the mineral or litter layer, and $A_{i(fine)}$ and $A_{i(coarse)}$ reflect their respective mass activities [Bq/kg]. The grid site inventory (I_T; Bq/m^2) reflects the combined activity of the size fractions within both litter layer and mineral soils, accounting for their relative assumed densities and thicknesses:

$$I_T = \sum(A_{i,T} * \rho_i * h_i), \qquad \text{(Equation 2)}$$

whereby, ρ_i is the sample density (mineral soil 1400 [kg/m^3]; litter 500 [kg/m^3]), h_i = is the thickness of the associated layer or horizon [m]. We explore the effects of particle size, organic matter (here, litter layer), topographic setting, and forested or non-forested setting on retention or loss of FRNs by exploring how measured inventories are partitioned by size fraction and soil composition; where each product in the summation from Equation 2 is referred to as a component inventory (>2mm and <2mm for both litter layer and mineral soil layer). Total site inventories (I_T) allow us to then broadly compare total nuclide abundance across forested and non-forested systems. For auger inventories, only the <2mm size fractions were measured to inform on inventories. These auger data were used to assess if soils beneath 20cm contained significant FRN activity.

Determining Landscape-Scale Soil and Rock Cover

Grid-based collection and measurement of FRNs along with soil cover and thickness (described above) lends insight into meter-scale soil transport and storage. By collecting multiple data points within forested and non-forested systems, we attempt to understand system-wide patterns in soil transport and storage. Because these meter-scale

measurements are bias to soil dominated portions of the landscape (Figure 2), we require an independent method to assess soil and rock cover at a landscape scale.

Previous work in our study region has shown that coarse spatial resolution (30m) landcover data is useful in classifying basin-scale rock extent (Benjaram, 2017). However, finer resolution classification (10^0 – 10^2m) is required for determining the local distribution of bedrock and its controls, which are the focus of this study. Our study aims to quantify bedrock and soil cover in forested and non-forested areas of our study region, and we anticipated more extensive areal soil cover in forested regions. High-resolution imagery can be used to classify soil and rock cover across non-forested hillslopes, however, in forested areas, we required a method able to see beneath the canopy. Prior work has shown topographic steepness and/or roughness are correlated with rock cover in mountainous settings (Dibiase et al., 2012; Milodowski et al., 2015b). Thus, we combine both aerial imagery and high-resolution topography from LiDAR data, to understand and quantify patterns of soil cover and storage, and to test relationships with topography.

Remote Sensing Analysis

We use the National Agriculture Imagery Program (NAIP) dataset (USDA Farm Service Agency, 2015) (Figure 2) because of its spatial resolution (1m), spectral properties (blue, green, red, and near-infrared bands), and date of capture close to date of field work. This dataset is the basis for our classification of forest, soil, and rock cover.

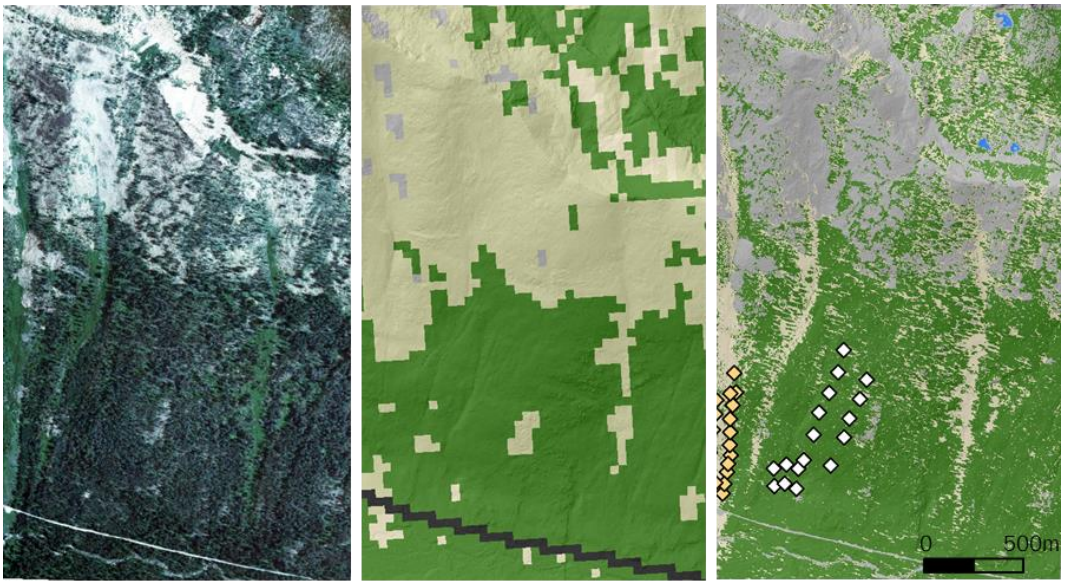

Figure 2. The subsample NAIP tile region (left) used to produce a landcover classified map. The near-infrared band (not shown) was used to improve vegetation type (herbaceous and conifer) classification. The 'Ohio Slide' is to the extreme west. National Landcover Database (2016) simplified class map (middle) showing accuracy of conventional 30m pixel size vs 1m NAIP classified map (right; orange are non-forest sites and white are forest sites). Landcover classes: forest (green); soil (tan); rock (grey); open water (black); roadway (black).

The NAIP tile was clipped to the south-facing slope in Lost Horse Creek to minimize spectral differences caused by multiple aspects. We used the Maximum Likelihood Classification tool (Spatial Analyst) in ArcGIS to produce a land cover map (Alibrahim, 2016). Maximum likelihood classification uses a spectral signature file of defined landcover class training fields and assesses the probability of a pixel's class assignment based on means and variances of training field values. Errors in maximum likelihood classification arise if classes overlap when the algorithm must assign a pixel.

In the NAIP region we use four land classes (rock, forest, grass/soil, and water) to define forested and non-forested rock and soil cover. Forested area is dominated by conifer cover and non-forested area is comprised of rock, soil, and vegetation (sparse

alpine larch, but dominantly low-lying herbaceous beargrass). Differences in these two classes of vegetation (conifer forest and herbaceous non-forest) are most pronounced in the near infrared spectrum where conifer reflectance differs from herbaceous reflectance, allowing for differentiation of vegetation classes in multispectral space (Campbell and Wynne, 2011). Each landcover class contained 35 training fields and each training field exceeded 40 (10 * n spectral bands, where n = 4 here) homogenous pixels (Congalton, 1991). Training fields were selected based on homogenous pixels that ideally represent the landcover class of interest. To ensure accuracy and homogeneity in training field selection, we used multiple ancillary datasets: on-ground familiarity with the field site, high resolution (10 cm) aerial imagery, and histogram/scatterplot visualizations. Training fields were combined for each landcover class to create a distinct population of pixel spectral properties in histograms and scatterplots that uniquely identify each landcover class. Once we achieved a desired level of accuracy in the landcover map we passed the map through a 3m-centered majority smoothing filter to reduce noise (Milodowski et al., 2015b).

Iterative validation and refinement was done on the landcover map to achieve an error of less than 5% based on confusion matrices that yield overall accuracy. Confusion matrices assess overall accuracy and misclassification by assessing manually classified misidentified pixels (i.e.: whether a manually identified forest pixel corresponds with a NAIP forest classified map pixel; for further details see Appendix B).

Topographic Analysis

Topographic analyses were used to understand variability in slope, elevation, and roughness and how they relate to soil distribution in non-forested and forested regions. Prior work in mountainous systems identified that rock cover may correlate with slope angles beyond some threshold or with fine-scale topographic roughness (Dibiase et al., 2012; Dietrich and Perron, 2006; Milodowski et al., 2015b). We combined these rock exposure analysis techniques using a 1m resolution LiDAR dataset. We compared non-forested rock and soil cover determined from the NAIP landcover map to hillslope gradient and roughness, calculated as the standard deviation of slope over a 3m window (SDS). These methods allowed us to assess topographic indicators of rock and soil cover in non-forested regions of our study site.

Using the NAIP classified map, we tested SDS roughness thresholds that are predictive of non-forested NAIP rock exposure and NAIP soil. The goal was to identify an SDS roughness value above which ‘rough’ pixels correlate with rock cover, and below which ‘smooth’ pixels correlate with soil cover. Multiple potential SDS roughness thresholds were compared to understand the trade-off between accurate and in-accurately predicted rock and soil pixels. We then quantified true positive rate (NAIP rock pixels above SDS threshold), false positive rate (NAIP soil pixels above SDS threshold), overall landscape accuracy (sum of NAIP rock above threshold and NAIP soil below threshold), and maximum accuracy in rock identification (the rate of NAIP rock above threshold). These quantified assessments allowed us to identify SDS roughness values that yield both the highest confidence in rock exposure identification (maximum accuracy) and the

highest confidence in non-forested pixel classification to soil and rock using roughness (overall accuracy). These estimates are found to be conservative indicators of rock exposure (Milodowski et al., 2015b). Using this method, we conservatively quantified extent of rock cover in the non-forested region, and then applied these calibrated SDS thresholds to the forested system where satellite (NAIP) remote sensing data is obscured by canopy cover to provide landscape rock exposure insight.

Statistical Analysis

We performed statistical analyses using the Mann-Whitney-Wilcoxon Test which tests whether independent distributions are identical, without assuming normal distribution of data. This is used to test independence between forested and non-forested soil cover, soil thickness, and FRN inventories. Correlation was also tested between topographic variables (slope, planform curvature, profile curvature, and elevation at a 3m window around each site) and local field sample findings (soil cover, soil thickness, and maximum soil depth in forested and non-forested systems). These correlations are presented using linear regression correlation coefficients (R) and associated p-values.

RESULTS

Fallout Radionuclide Analysis

Fallout radionuclide analyses reveal soils in forested and non-forested systems have distinct variability in $^{210}Pb_{ex}$ and ^{137}Cs inventories (Table 1). $^{210}Pb_{ex}$ inventories are higher in the forested system (15.49±1.91 kBq/m^2, excluding outliers) compared to non-forested $^{210}Pb_{ex}$ inventories (10.45±0.97 kBq/m^2, excluding outliers; Figure 3), supported by Mann-Whitney-Wilcoxon Test results ($p = 0.04$). ^{137}Cs average inventories and variability are not meaningfully different between forested and non-forested systems (3.73 ± 0.42 kBq/m^2 and 4.04 ± 0.34 kBq/m^2 respectively, excluding outliers; $p = 0.93$; Figure 3b). The difference in $^{210}Pb_{ex}$ and similarity in ^{137}Cs inventories between systems results in the ratio of $^{210}Pb_{ex}$: ^{137}Cs being higher, on average, for forested inventories (4.0±0.4) than the ratio for non-forested inventories (2.7±0.2).

	Component Inventory [kBq/m2]								Inventory [kBq/m2]	
	<2mm				>2mm				Site Total	
Site	$^{210}Pb_{ex}$ †	^{137}Cs †	$^{210}Pb_{ex}$ ‡	^{137}Cs ‡	$^{210}Pb_{ex}$ †	^{137}Cs †	$^{210}Pb_{ex}$ ‡	^{137}Cs ‡	$^{210}Pb_{ex}$	^{137}Cs
F1	11.81	6.25	4.80	0.68	7.57	1.89	4.32	0.50	28.50	9.32*
F2	3.43	1.91	6.74	2.04	2.85	0.83	6.35	1.34	19.37	6.12
F3	0.59	0.87	1.63	0.34	0.15	0.21	1.02	0.18	3.39	1.60
F4	1.14	1.54	2.84	0.79	ND	ND	ND	ND	(3.99) 10.40	(2.32) 3.41
F5	2.97	1.46	5.43	0.97	2.91	1.49	7.65	0.68	18.96	4.61
F6	4.85	1.89	4.91	0.99	0.00	0.43	7.09	1.17	16.85	4.48
F7	0.30	0.53	4.98	0.49	0.08	0.05	2.18	0.14	7.53	1.21
F8	4.95	2.89	2.80	0.38	0.15	0.16	2.43	0.14	10.33	3.58
F9	2.06	0.89	12.23	2.98	0.19	0.07	7.29	0.77	21.77	4.71
F10	0.27	0.34	8.29	1.38	0.24	0.06	9.31	1.16	18.10	2.94
F11	2.00	0.91	10.89	2.19	0.65	0.16	9.42	2.12	22.96	5.37
F12	0.50	0.91	14.16	3.51	0.10	0.02	6.29	0.62	21.05	5.06
F13	2.88	1.26	5.21	0.93	0.18	0.07	1.29	0.16	9.57	2.42
F14	3.28	2.54	1.86	0.34	0.98	0.29	2.44	0.12	8.56	3.29
F15	6.09	3.89	4.11	1.18	1.10	0.44	0.98	0.69	12.28	6.20
F16	3.99	1.38	5.13	0.51	0.72	0.29	15.97	1.04	25.82	3.22
F17	1.08	0.97	0.94	0.16	0.20	0.03	0.53	0.03	2.74	1.19
Average	3.07	1.79	5.70	1.17	1.13	0.41	5.28	0.68	15.49	3.73
Std. Error	0.44	0.34	0.88	0.23	0.47	0.13	1.02	0.14	1.91	0.42
Site	$^{210}Pb_{ex}$ †	^{137}Cs †			$^{210}Pb_{ex}$ †	^{137}Cs †			$^{210}Pb_{ex}$	^{137}Cs
NF1	10.80	3.02			5.35	1.77			16.15	4.79
NF2	6.03	1.38			0.09	0.28			6.13	1.66
NF3	4.86	2.18			1.01	0.39			5.87	2.57
NF4	5.88	2.85			2.49	0.81			8.37	3.66
NF5	7.83	3.68			0.96	0.77			8.79	4.45
NF6	5.75	3.70			0.18	0.36			5.93	4.06
NF7	7.84	2.83			0.21	0.20			8.05	3.03
NF8	6.60	2.96			0.08	0.20			6.67	3.16
NF9	7.46	3.50			0.58	0.48			8.04	3.99
NF10	8.86	3.91			5.05	1.46			13.91	5.38
NF11	9.32	3.54			8.56	3.36			17.88	6.90
NF12	8.71	2.19			4.20	0.46			12.91	2.64
NF13	10.80	5.50			0.84	0.50			11.63	6.00
NF14	10.53	2.96			1.81	0.37			12.34	3.33
NF15	8.16	3.34			0.30	0.16			8.46	3.50
NF16	18.75	7.83			10.90	0.88			29.65*	8.71*
NF17	9.35	3.30			1.59	0.36			10.94	3.66
NF18	17.66	6.63			1.92	0.29			19.58	6.92
NF19	6.47	2.80			0.02	0.24			6.49	3.05
Average	9.03	3.58			2.43	0.70			10.45	4.04
Std. Error	0.82	0.34			0.69	0.17			0.97	0.34

Table 1: † mineral soil component; ‡ litter layer component for $^{210}Pb_{ex}$ and ^{137}Cs inventories for forested (F) and non-forested (NF) sites. *Forested site F4 did not have sufficient coarse particle sample to be measured.

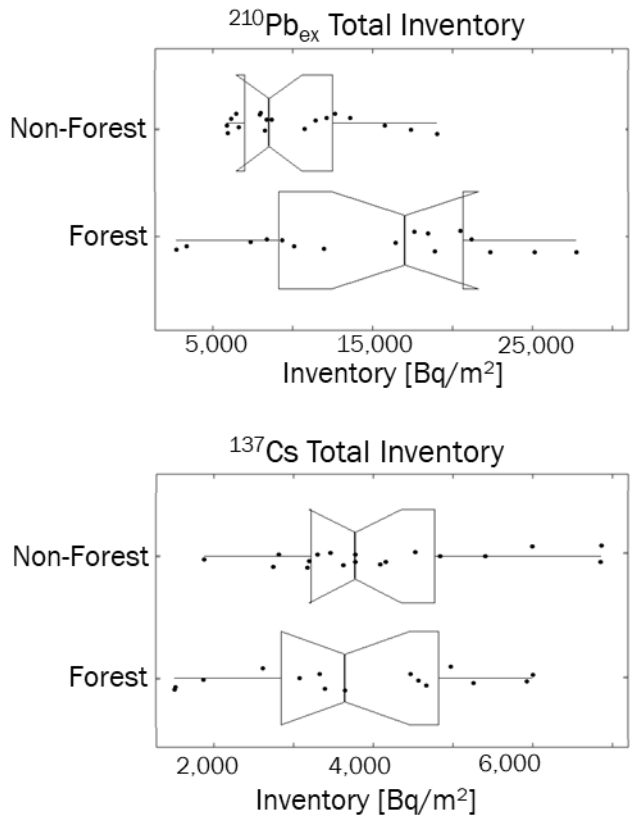

Figure 3: Forested and non-forested soil FRN inventories [Bq/m^2] compared using notched box plots where notches represent the 95% confidence interval about the median, and box extents delineate interquartile range. Forested soils (n = 16) display more variable, and higher average and median $^{210}Pb_{ex}$ (top) than the non-forested system (n = 18, excluding 1 outlier). ^{137}Cs (lower) has similar averages and variability for both systems.

Total site inventories reflect the contribution of multiple soil components, including mineral and organic horizons, and coarse and fine particle fractions. These component inventories uniquely contribute to total site inventories (Figure 4). Mineral soil component inventories show similar behavior whereas the litter layer component is enriched in $^{210}Pb_{ex}$ (Figure 5). However, litter layer contributions to total activity (Bq/kg) is large, and relative contribution to total inventory (Bq/m^2) is decreased when the litter layer's low density is accounted for (Equation 2; Figure 5). In the forested system, an

average of 71±12% of the $^{210}Pb_{ex}$ and 49±10% of the ^{137}Cs total site inventory is contained within the litter layer (Figure 4A), while mineral soils contribute the remaining inventory. Because the litter layer is absent in non-forested soils, this results in significantly different mineral-soil component inventories of $^{210}Pb_{ex}$ in the forested and non-forested systems (4.20±0.91 and 10.45± 0.97 kBq/m^2 respectively; Figure 4A: "Forested mineral" vs "Non-Forested total"). Non-forested component inventory is instead attributable to differences in mineral soil particle size inventories, which is also observed in the forested components. The <2mm mineral soil component (<2mm$_{forest}$ = 3.07±0.44 kBq/m^2; <2mm$_{non\text{-}forest}$ = 9.03±0.82 kBq/m^2) contributes to $^{210}Pb_{ex}$ total inventory more than the >2mm component (>2mm$_{forest}$ = 1.13±0.47 kBq/m^2; >2mm$_{non\text{-}forest}$ = 2.43±0.69 kBq/m^2). Whereas, both particle size components of the forested litter layer have equivalent average $^{210}Pb_{ex}$ inventories (>2mm = 5.70±0.88 kBq/m^2; <2mm = 5.28±1.02 kBq/m^2). ^{137}Cs inventories do not show the same patterns for the litter layer, but the mineral soil <2mm particle size inventories behave similarly to the $^{210}Pb_{ex}$ mineral soil particle size inventories (Figure 5).

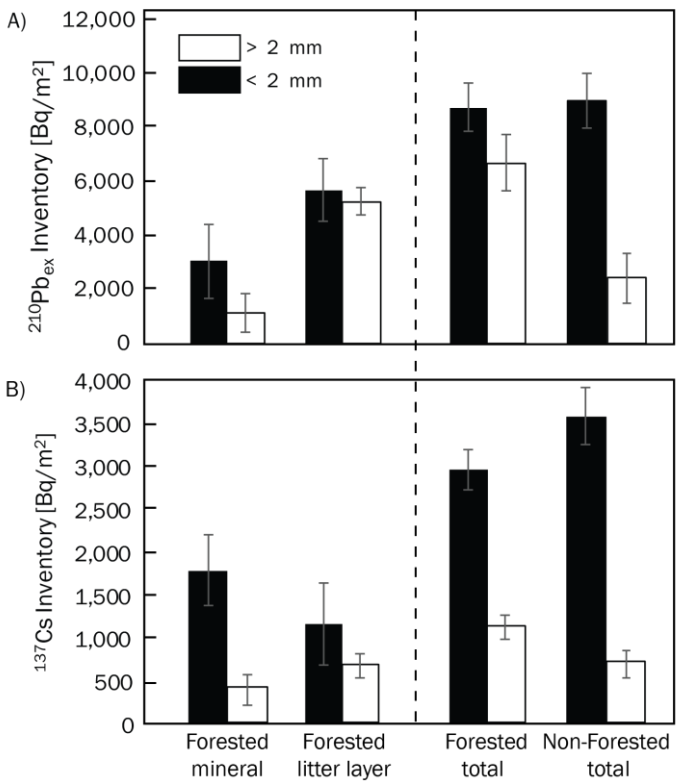

Figure 4: $^{210}Pb_{ex}$ (a) and ^{137}Cs (b) component inventories for forested and non-forested sites. A): Total inventories reflect sum of respective components for each system (15.49±1.91 kBq/m^2 for forest and 10.45±0.97 kBq/m^2 for non-forest). Litter layer comprises 71±12% total $^{210}Pb_{ex}$ inventories on average. (b) ^{137}Cs does not show the particle size differentiation seen in the litter layer $^{210}Pb_{ex}$ inventories. Contribution to total inventory is also equivalent for the litter layer and mineral components.

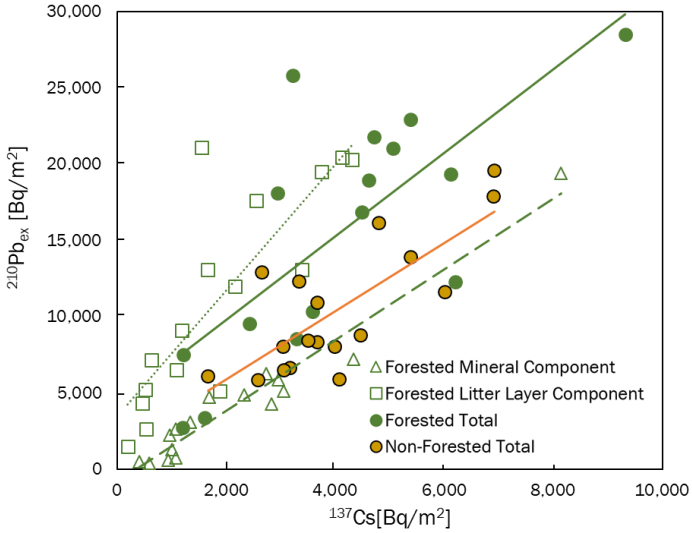

Figure 5: Total $^{210}Pb_{ex}$ and ^{137}Cs inventories are coupled, such that sites with high $^{210}Pb_{ex}$ generally have high ^{137}Cs, however this relationship is distinct between forested (solid green line; $r^2 = 0.55$) and non-forested systems (solid orange line; $r^2 = 0.60$). Non-forested inventories are generally $^{210}Pb_{ex}$ depleted compared to forested inventories, resulting in distinct ratios of $^{210}Pb_{ex}$ to ^{137}Cs and (y_{forest} intercept=4.28 kBq/m^2 & $y_{non\text{-}forest}$ intercept=-1.02 kBq/m^2).

Auger depth samples were measured for FRN inventory to investigate whether the surficial sampling methodology truncated FRN profiles and if deeper samples contained significant activities. We measured <2mm samples in the 20cm increment augers. In non-forested areas, the upper 20cm sampling captured 96±2% of total $^{210}Pb_{ex}$ inventories, and 93±3% of ^{137}Cs. In the forested system, the upper 20cm sampling captured slightly less, totaling 85±5% of $^{210}Pb_{ex}$ and 83±6% of ^{137}Cs (Figure 6).

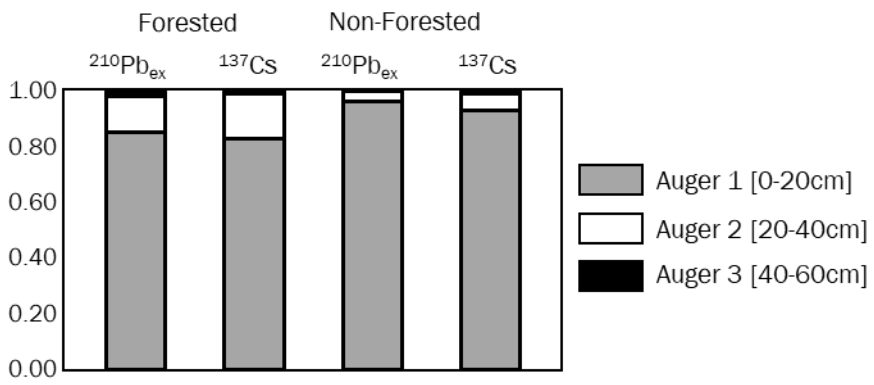

Figure 6: Percent contribution to total FRN inventories from auger samples (0-20cm, 20-40cm, and 40-60cm segments). Auger 1 contributions dominate the total soil inventory and contain approximately an order of magnitude more FRNs than auger 2 contributions. Soils deeper than 40cm (auger 3) contribute less than 3% to total inventories across the landscape.

Local Spatial Scale and Topographic Findings

Field observations and sample collection from 1m grid sites inform us on local spatial scale and local topographic differences, specifically quantification of rock cover, soil cover, and soil thickness at a sub-meter spatial scale. Rock cover in both forested and non-forested systems consists of talus, boulders, and stepped bedrock features. However, soils differ between the two systems, the primary difference being the presence of a surficial litter layer in the forested system. Field data can be found in Appendix C.

We find median percent soil cover for forested sites (94.4%±2.6%, n = 17) is higher than non-forested sites (88.3%±1.9%, n =19) (Figure 7; Mann-Whitney-Wilcoxon Test, p = 0.027). However, measured average and maximum soil thicknesses between systems are similar (p = 0.358 & 0.188, respectively). Importantly, because surface sampling design stopped at 20 cm depth, these ‘averages’ underestimate actual soil depths and variability. Using all depth data from soil grids, we find forested grids on

average have a greater frequency of thicker soils (≥20cm; 47%, n =154) than non-forested grids (27%, n = 171).

We also compare relationships between local soil cover, average soil depth, and maximum soil depth with topographic variables (local slope, planform curvature, profile curvature, and elevation using a 3m window; Figure 8). Seven pairs of variables displayed a moderate to strong correlation (R>0.3) whereas 27 pairs had weak to no level of correlation (R<0.3). Forested system correlations include average soil depth with slope (R=-0.49), maximum soil depth with elevation (R=0.50) and slope with elevation (R=0.83). Non-forested correlations include average soil depth with elevation (R=-0.55) and slope (R=-0.38), percent soil cover with elevation (R=-0.6), and slope with elevation (R=0.44).

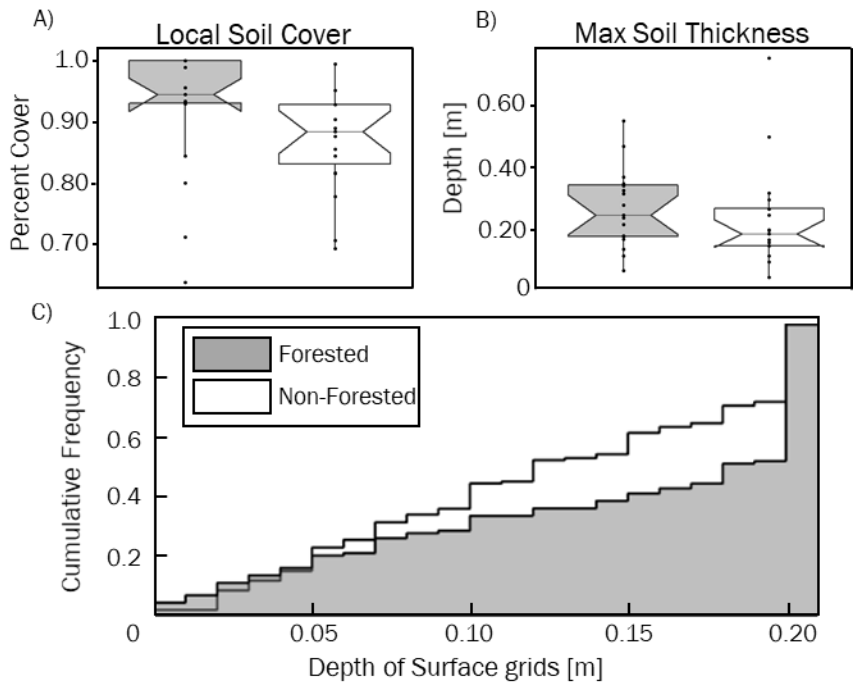

Figure 7: Fine scale ($1m^2$) soil distribution between forested (grey; n = 17) and non-forested (white; n= 19) systems. (a) Local soil cover determined with $1x1m^2$ grids is higher in forested sites (p = 0.03). (b) Max soil thicknesses are also not distinct (p=0.49). (c) Cumulative frequency distribution: 47% of forested samples are ≥20cm and 27% of non-forested samples are ≥20cm. Median soil thickness is forest is 0.18m and 0.12m for non-forest.

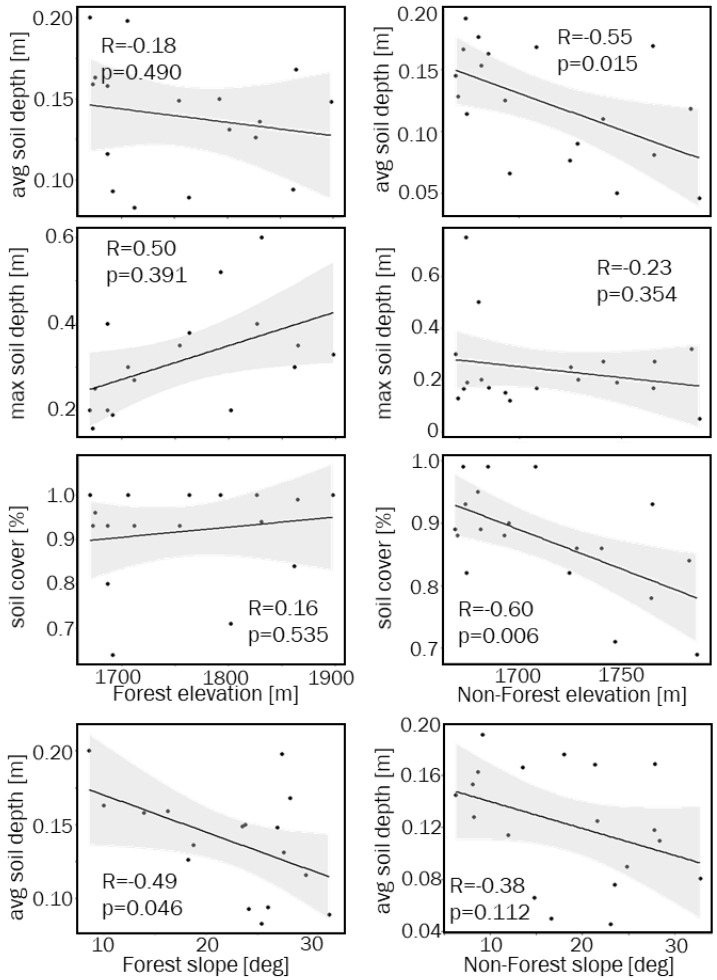

Figure 8: Linear regressions for different soil and topographic properties within forested and non-forested slopes. Grey swaths reflect the 95% confidence intervals. Topographic regressions of elevation and slope not shown (forest: R=0.83, p=0.0001; non-forest: R=0.44, p=0.080).

Rock and Soil Classification

Non-Forested Rock and Soil Delineation Using Geospatial Products

We used 1m-resolution NAIP imagery to classify pixels as soil, rock, and forest cover classes (Figure 2). Confusion matrices that compare correctly and incorrectly classified rock, soil, and forest pixels showed an accuracy of only 37% for the first

classified map product. This accuracy was increased to 97% through iterative refinement of training classes, particularly border pixels of forest and soil where a majority of errors occurred due to the similarity in spectral responses of the vegetation classes. Importantly, NAIP defined soil and rock classes only apply to the non-forested system, because they cannot be observed beneath forest canopy.

NAIP-derived landcover classes have distinct and subtle slope distributions, with rock classes occurring at higher mean slope angles (29.63±0.01º) compared to both soil (25.92±0.02º) and forest (23.01±0.02º) classes. Within the non-forested areas (soil and rock NAIP classes) we find a transition in rock and soil cover at slopes between 24-42º. Across this threshold, soil cover notably decreases from 40% to below 20%, while rock cover increases from 60% to over 80% (Figure 9).

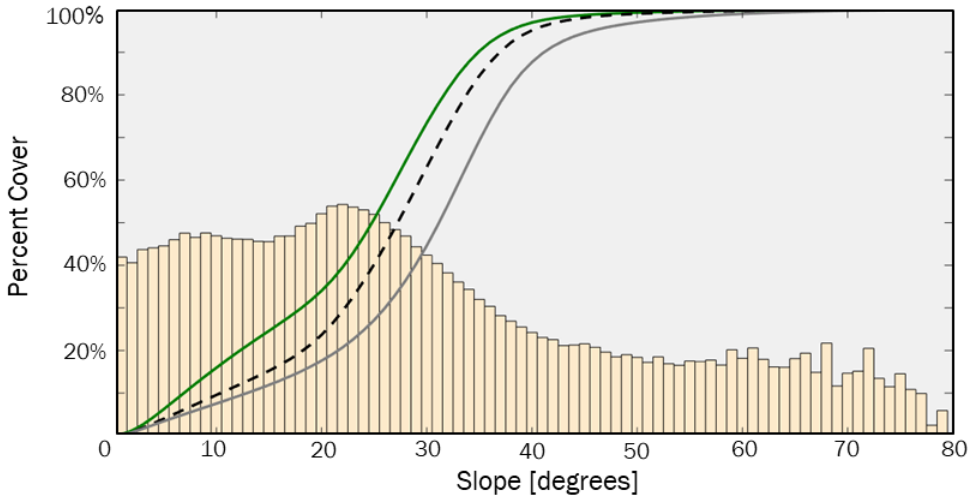

Figure 9: The proportion of NAIP classified soil (tan) and rock (grey) landcover with hillslope angle (1º bins) in non-forested regions of the study area. Cumulative frequency distribution curves of slope for forest (green), rock (grey), and soil (dashed black). We find a notable decrease in soil cover at slope angles between 24-42º, whereby rock persists at 80% of the landcover on steep slopes. Importantly, this plot only shows fractional persistence of rock and soil classes at each topographic position and does not communicate the overall abundance, which is shown by the cumulative distributions curves for slope gradient. Here, the area occupied by >40º slopes represents 11.4% of all non-forest cover and 3.5% forest cover data across the study region.

We explored whether rock and soil cover are identifiable by topographic roughness (e.g., Milodowski et al., 2015b) using standard deviation of slope. The assumption underlying roughness analysis is that rock outcrops are associated with topography above some roughness threshold, while soil cover generally is found in smooth regions below threshold. High angle portions of the study area are notably rougher (>45º; SDS = 5.35±0.03º) based on SDS analysis than low slope (< 35º; SDS = 2.65±0.00º) regions. We tested if roughness thresholds independent of slope angle could be used to accurately identify rock exposure. Testing multiple thresholds, we found that as the roughness threshold (SDS value) increases, there is a tradeoff between the fraction of correctly defined NAIP rock (true positives; where NAIP rock is above the SDS

threshold) and correctly defined NAIP soil (true negatives; where NAIP soil is below the SDS threshold) classes (Figure 10). The true positive rate (rate of correctly identified rock) rapidly decreases, but at a slower rate than that of false positives (rate that identifies soil pixels as above threshold) (Figure 10a). Highest overall accuracy occurs at an SDS > 3º (59.4%), maximizing both the number of rock-classified pixels above this threshold and the number of soil-classified pixels below threshold (Figure 10b). Overall accuracy averages the rate of true positives and true negatives, and therefore weights the accurate classification of land-cover pixels equally, despite their disparate abundance on the landscape. This SDS value of 3º minimizes incorrectly assigned soil pixels to rock (false positive rate: 22%) while correctly assigning rock pixels to above threshold (true positive rate; 41%). At an SDS > 3º, areas defined above threshold are approximately 74% rock (Above-threshold % rock; Figure 10c). While overall accuracy focuses on the correct classification of both rock and soil cover, we determine the maximum accuracy occurs at SDS > 6º, maximizing the percent rock that occurs above SDS threshold (79.1%; Figure 10c).

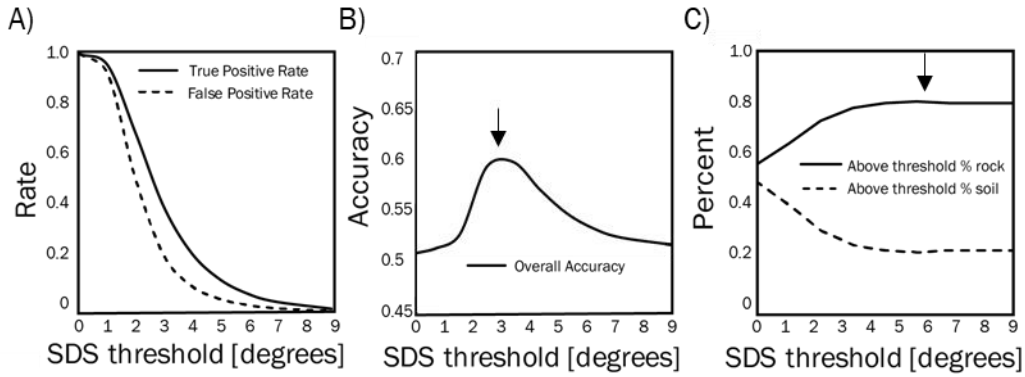

Figure 10: SDS values were compared to NAIP landcover classes to test if roughness thresholds predict rock and soil cover. (a) True positive (rock above threshold) and false positive (soil above threshold) rates both decrease as the selected SDS threshold increases. (b) Overall accuracy is determined as the combined rate of rock pixels above threshold and soil pixels below the selected threshold. The greatest overall accuracy (59.4%) occurs at an SDS=3º, where we maximize true positives while minimizing false positives. (c) Maximum accuracy prioritizes rock categories, where above threshold roughness values correspond to rock classes, and is highest at SDS>6º, where 79.1% of pixels are rock cover.

Roughness metrics identified two thresholds of rock cover (SDS 3º and 6º) corresponding to the values with the greatest overall accuracy (59.4%) and maximum accuracy (79.1%) of rock classification in non-forested areas. We used these thresholds to identify two types of rock cover: low relief and high relief rock exposures. We label low relief rocky exposures as Rock Type 1, between an SDS of 3-6º, and describe high relief rock exposure as Rock Type 2, at an SDS>6º. Rock Type 2 is readily identified using field data (Figure 11).

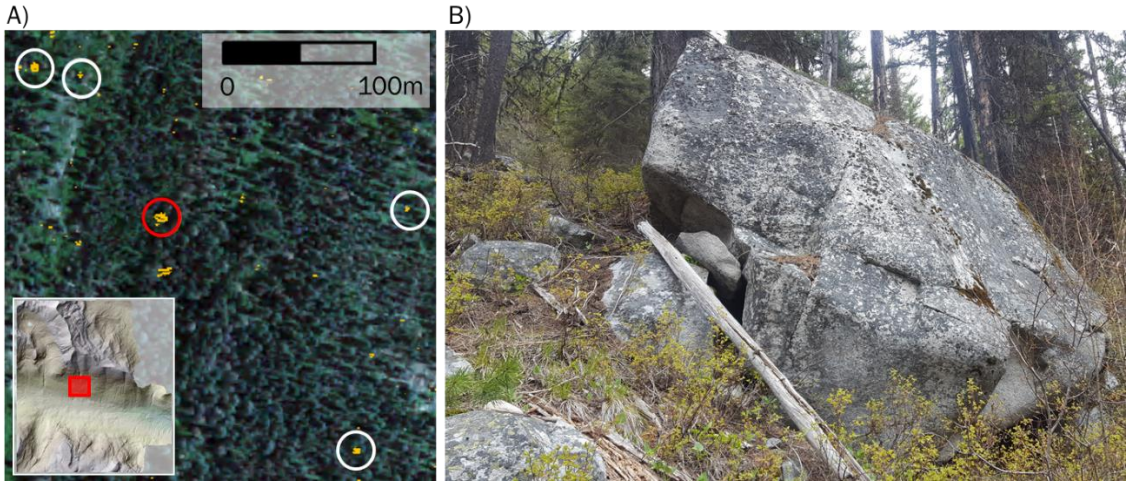

Figure 11: (a) Regions with SDS>6º (orange) are highlighted by white rings. The extent of this aerial photo is shown by the inset map. (b) Each of the circled sites were field-validated as large boulders or outcrops of high relief (Rock Type 2). The boulder in the photo corresponds to the red circle in (a).

Delineation of Rock and Soil Classes Under Forest Cover

We used defined SDS thresholds of 3º (Rock Type 1) and 6º (Rock Type 2) from non-forested regions to estimate rock and soil cover areas in the forested NAIP class, where canopy obscures ground cover (Figure 12; Table 2). Because of the different areal extents of forested and non-forested systems, we compared estimates of rock cover as the ratio of the SDS above threshold area divided by the sum of all pixels within the region of interest (θ_{SDS}; Table 2). Here, higher θ_{SDS} values indicate more extensive roughness-predicted rock cover. Based on this analysis, forested regions exhibit roughly half the rock cover of non-forested regions for both Rock Type 1 (SDS=3º; $\theta_{SDS,\ forested}$=0.20; $\theta_{SDS,\ non\text{-}forested}$=0.34) and Rock Type 2 (SDS=6º; $\theta_{SDS,\ forested}$=0.02; $\theta_{SDS,\ non\text{-}forested}$=0.05).

	Forested SDS thresholds		Non-Forested SDS thresholds	
	3º	**6º**	**3º**	**6º**
Above Threshold [m^2]	262,000	32,700	343,000	58,700
Below Threshold [m^2]	1,070,000	1,300,000	671,000	955,000
θ_{SDS}†	0.20	0.02	0.34	0.05

Table 2: SDS roughness classified rock cover under NAIP defined forest and NAIP defined non-forest † θ_{SDS} = SDS above threshold pixels/ total SDS defined area at threshold.

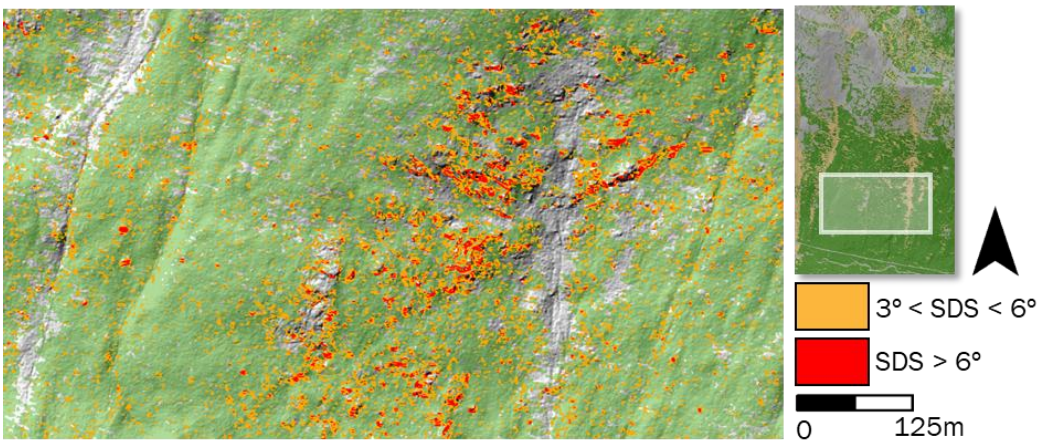

Figure 12: SDS defined roughness in forested system; Rock Type 1 (SDS 3-6º) and Rock Type 2 (SDS>6º). Non-forested areas (appearing as hillshade) corresponding roughness areas are not shown. There is a large extent of rock exposure centered in the figure; aside from this feature only sporadic and relatively small areas of SDS defined rock cover occur below the forest canopy.

DISCUSSION

Calibration and Application of Fallout Radionuclides in a Mountain Setting

Application of fallout radionuclides (FRNs) as tracers of soil transport and storage in forested mountain systems requires establishing a unique methodology. We used grid-based, integrated sampling to account for local variability in FRNs, and separated mineral and organic horizons and size fractions to understand how nuclides are partitioned both within soils and across the landscape. Our data, from 37 sites, provide some new insights into the behavior of fallout radionuclides in mountainous soils and how they can be used to understand soil residence and erosion in these systems.

Firstly, we found that measuring nuclide activities in organic rich horizons and in coarse soil particles was necessary to measure total nuclide inventories. We found that the coarse mineral fraction of soils accounted for ~15% of soil $^{210}Pb_{ex}$ and ^{137}Cs inventories. Additionally, in forested regions of our study, $^{210}Pb_{ex}$ activities in organic layers are an order of magnitude higher than in underlying mineral soil (530±49 and 42±10 Bq/kg, respectively). On average, the litter layer accounts for ~70% of total soil $^{210}Pb_{ex}$ inventories. That the upper soil horizon has higher activity (and inventory) is not in-itself surprising, since we would expect the highest activity of FRNs at the surface (Walling et al., 1995; Teramage et al., 2014). However, the litter layer also contains a surprisingly large contribution from coarse material (>2mm diameter). The coarse organic matter accounts for over a third of the $^{210}Pb_{ex}$ inventory in forested sites.

These findings for $^{210}Pb_{ex}$ contrast with those of ^{137}Cs, which was primarily concentrated in mineral soils, with litter layers only contributing ~29% to total ^{137}Cs

inventories (<2mm=11%; >2mm=18%). These findings reinforce prior work suggesting that $^{210}Pb_{ex}$ and ^{137}Cs strongly sorbs to organic matter, in turn following the particles through the system in addition to fine soil particles (Dörr, 1995; Dorr and Munnich, 1989; Wakiyama et al., 2010). ^{137}Cs's transport is further complicated by enhanced chemical exchange processes in mineral soil horizons resulting in variable transport when compared to $^{210}Pb_{ex}$ (Dorr and Munnich, 1989; Dörr and Münnich, 1991).

The fact that coarse organic particles (>2mm) are major components of recorded inventories suggests that the concentration of FRNs during litter production may be important in forested systems (Dörr and Münnich, 1991; Teramage et al., 2014). This is reinforced by findings that suggest organic matter found in the organic horizon is important in considering total FRN inventory (He and Walling, 1996), however these studies do not include particles larger than 2mm and rarely assess superficial litter (Teramage et al., 2014; Wakiyama et al., 2010; Yang and Appleby, 2016). Because we find FRNs are concentrated in the surficial litter layer, sub-surface organic and mineral soil inventories are directly affected by litter production, litter turnover, and decomposition rates of litter. In combination, these findings indicate the measurement of forested FRN inventories requires consideration of litter layer, litter's turnover rate and cycling of FRN to soils, and coarse particle components to accurately interpret net erosion and deposition patterns of sediment on forested mountain hillslopes.

Delineating Soil Cover Using Remote Geospatial Data

Iterative classification of aerial imagery was highly powerful and accurate in our determination of soil cover in non-forested regions (97% overall accuracy; Figure 2).

However, we found mixed success in comparisons of topographic metrics with soil and rock cover. Using SDS roughness thresholds (SDS>3º), we only achieve 59.4% overall accuracy identifying landscape soil and rock cover (Figure 10). These findings indicate that accuracy of rock cover identification is low at a landscape-scale. However, specific identification of rock cover increases to a maximum accuracy of 79% (SDS>6º) using roughness. Importantly, maximum accuracy only identifies 3.9% of landscape pixels as rock cover with 79% maximum accuracy meaning a majority of the landscape (96.1%) is defined as soil.

Though we find questionable success in soil and rock classification at a landscape scale, we find that topographic variability across our study site is correlated to important changes in soil and rock cover. In non-forested regions where soil and rock classification are accurate, we observe a doubling in rock cover as slope gradients increase from 24º to 42º (Figure 9). This transition is not binary however, and we still find significant soil cover even at the highest slope angles (>42º), such that soils are persistent and resilient in steep landscapes typically thought of as bedrock dominated (Dibiase et al., 2012). Furthermore, roughness thresholds were sensitive to different forms of rock cover, and Threshold 2 (SDS>6º) was field validated to represent large, high-relief boulders (Rock Type 2), while Threshold 1 (SDS 3-6º) captured smooth or stepped bedrock topography (Rock Type 1). Overall soil and rock classification using these thresholds was low however, due to fact that other bedrock surfaces were found at very low roughness values (SDS<3º). That bedrock has many different forms in this system is important since these morphologies influence weathering and erosion processes. High relief rock exposure

provides more surface roughness that may act akin to vegetation damming of uphill soils (Dibiase and Lamb, 2013), while low relief rock is subject to surface transport processes like sheet flow that may enhance particle transport and erosion (Robichaud et al., 2010).

Soil Distribution on Mountain Hillslopes

Our data span multiple scales and methodologies, and provide repeated and consistent evidence that forested hillslopes have more extensive and thicker soils, with longer residence times and different erosion processes, compared to topographically-similar hillslopes lacking forest cover. Here, we highlight the data that support these conclusions, acknowledge important caveats, and challenge assumptions inherent in our interpretations.

Firstly, we find that soil thicknesses, measured in our local grid-based sampling design are higher in forested regions than non-forested (6cm median difference). Though these systems are only ~6cm different, this is noteworthy considering most soils are thinner than 20cm (53% and 73% in forested and non-forested systems respectively; Figure 7). This difference in soil thickness may be partially, but not entirely, due to the presence of a litter layer in the forested system, which averages 4±2cm in thickness. However, we also find significant differences in soil cover at a local scale, such that soil grids in forested regions contained 6% less rock cover than grids at similar topographic positions in the non-forested system. Soil cover differences are less likely to be solely attributed to litter cover since all grids observed here contained mineral soil beneath litter layers. This may be the result of geochemical feedbacks between litter and soil supporting the cooccurrence of the two layers (e.g. Xiong et al., 2014), as organic matter

may enhance water retention, weathering, and bioturbation in underlying layers. These findings thus highlight the importance of litter in soil dynamics on steep forested mountain slopes and show that vegetation influences soil storage.

Secondly, FRNs should provide insight into relative soil residence times across our study system, however the two nuclides examined here provide contrasting results. Our methodological design was predicated on the assumption that nuclide inventories should be positively related to soil residence times, such that higher FRN inventories in the forested system would suggest lower erosion rates than the non-forested system. Indeed, at a landscape scale, we find higher $^{210}Pb_{ex}$ inventories in the forested system than the non-forested system, suggesting longer soil residence times under forest cover. However, ^{137}Cs inventories are similar between systems. This is initially puzzling because these nuclides are thought to bind to soils and thus record erosion processes similarly (e.g. Zapata, 2012).

Several factors that may explain this disparity can be ruled out. While our sampling design focuses on the upper 20cm of soils, FRN analysis of auger measurements show that the upper 20cm contains on average ~84% of the FRN inventory in forested and ~95% FRN inventory in non-forested areas (Figure 6). Thus, differences in inventories cannot result from exclusion of deeper soils, and if they do, differences would only enhance the already higher forested inventories. Another possible explanation could be different FRN delivery and cycling in forested and non-forested areas. The non-forested system experiences increased avalanche activity upslope, and increased snowpack in lower slope positions (Gelfan et al., 2004; Kuz'min, 1960); these processes

would increase FRN delivery (e.g. Dörr, 1995) to the downslope regions in which we sampled. Importantly, this increased delivery should enhance FRN inventories in non-forested systems. Instead, we find less $^{210}Pb_{ex}$ and similar ^{137}Cs inventories compared to the forested system. In addition, the cycling of $^{210}Pb_{ex}$ in vegetation occurs on timescales short enough (<1000 days; Osaki et al., 2003; Teramage et al., 2014) to not influence the century-scale residence times of FRNs in the forested system. Therefore, we find limited evidence that FRN inventories observed here are dependent on the uptake, interception, or deposition of nuclides by vegetation. If avalanche mediated FRN delivery and FRN cycling within vegetation did influence FRN inventories, they would only enhance the disparity of FRN inventories we observe between forested and non-forested systems. Therefore, recorded inventories are highly conservative.

In summary, differences in FRN inventories are not attributable to deep FRN profiles not captured by sampling or to variable flux in each system. Different observed patterns in ^{137}Cs and $^{210}Pb_{ex}$ in forested and non-forested systems can instead be attributed to erosion processes. Importantly, each nuclide records erosion differently due to their disparate delivery mechanisms. $^{210}Pb_{ex}$ undergoes constant delivery, resulting in a peak activity closer to the soil surface (Appleby and Oldfield, 1978; Walling et al., 1995), while peak deposition of ^{137}Cs (ca. 1963) and subsequent downward migration in the soil column (He and Walling, 1997) results in a ^{137}Cs peak beneath the surface. This different delivery and partitioning of ^{137}Cs and $^{210}Pb_{ex}$ results in the former being potentially less sensitive to surface-specific erosion processes than $^{210}Pb_{ex}$ in certain settings (Walling et al., 2003). Thus, observed differences in $^{210}Pb_{ex}$ and similarity in ^{137}Cs inventories across

our systems are consistent with increased surficial erosion processes (e.g. rainsplash and runoff) in the non-forested system (Dorr and Munnich, 1989; He and Walling, 1997). What processes may explain these nuclide patterns? Higher interpreted erosion in the non-forested system may occur by a combination of increased overland flow, reduced shielding from rainsplash, and lack of biomass provided microtopographic roughness to inhibit downhill soil loss (Dibiase and Lamb, 2013; Marston, 2010; Roering et al., 2010). In the forested system, litter layer shielding and canopy interception of rainsplash, along with decreased surface runoff (Lowdermilk, 1930; Miyata et al., 2009) reduces the likelihood of surface erosion and enhances soil storage.

We specifically focus on hillslopes where vegetation patterns are persistent over the relevant timescales of our analysis (Bernhard, 1899). However, our observations of greater soil storage in forested areas have important implications for the systemwide disturbance regimes that influence vegetation and soil cover feedbacks across the region. Specifically, forest fires across the Bitterroot Mountains directly control the extent of forested biomass over multiple return intervals (Heyerdahl et al., 2011, 2014) and are highly sensitive to shifts in climate (McWethy et al., 2010; Whitlock et al., 2003). Though not explicitly explored here, we can provide hypotheses for how soil storage on these hillslopes may respond to disturbance if fire related erosion events control patterns in soil distribution.

High intensity fires have a return interval of approximately 100-250 years across similar regions of the inland Rocky Mountain west (Covington et al., 1994; Heyerdahl et al., 2014). These disturbances are thought to dramatically alter soil storage by reducing

forest stand density (e.g., Robichaud et al., 2009; Sankey et al., 2017). A conservative measure of this soil loss can be estimated based on our soil cover data in forested and non-forested areas. If disturbance reduces previously forested soil cover to the level of our non-forested areas, this would mean a 6% increase in local rock cover at a sub-meter scale. Assuming this occurs in the shallowest soils (the sixth percentile of grid-scale soil thickness; 2cm; Figure 7), we would calculate a minimum of 30 kilotons/km^2 (kt/km^2) of erosion during disturbance. This estimate increases if we also consider that forested areas of our study area have ~6cm greater soil thickness than non-forested areas. Erosion of this 6cm would provide an additional 60 kt/km2 of soil loss, summing to 90 kt/km^2. If we consider the longer return interval of disturbance (250 yrs; Heyerdahl et al., 2011), then this would mean fire driven erosion alone could result in a long term-erosion rates of ~240 mm/ky (~360 tons/km^2/y). Though only a back of the envelope calculation, this estimated, disturbance-driven erosion rate is reasonable considering rates across similar systems do not largely differ from this value (Portenga and Bierman, 2011; Robichaud et al., 2009).

Conclusions

We collect extensive soil cover and thickness data for mountainous hillslopes across two distinct vegetation regimes and couple these with decadal timescale analysis of soil storage from FRNs. Our research contributes geomorphic insights into the evolution of steep, dynamic mountain systems, and adds to the field of short-term erosion studies. Firstly, we test the application of fallout radionuclide tracers in steep, mountain landscapes, and find that nuclide partitioning is strongly influenced by coarse and

organic-rich soils. We show that litter layers and coarse soil fractions contain significant components of the total nuclide inventory, and must be accounted for. Secondly, we show that systems traditionally thought of as bedrock dominated have highly variable soil depths and soil cover. Secondly, we show that the local transitions from soil mantle to bedrock are not easily diagnosed by topographic metrics (e.g., slope and roughness), and such applications require extensive site calibration to identify rock exposure confidently. Though we find rock exposure correlates with steep and rough topography, multiple complex and competing variables at a local scale influence the resilience of soils in mountainous landscapes. Lastly, combining our field, isotope, and geospatial methods, we find repeat evidence of more extensive soil storage and lower erosion rates in forested regions, compared to topographically- and lithologically-similar slopes devoid of forest cover. Importantly, the Bitterroot Mountains are subject to high intensity fire activity that alters forest regimes. Considering we find systems with persistent forest cover have greater soil storage, fire disturbance may significantly contribute to, or even dominate soil erosion rates and associated flux of sediment to rivers, over long time scales.

REFERENCES CITED

Abrahams, A.D., Parsons, A.J., and Wainright, J., 1995, Effects of vegetation change on interrill runoff and erosion, Walnut-Gulch, southern Arizona.: Geomorphology, v. 13, p. 37–48, doi: 10.1016/0169-555X(95)00027-3.

Alden, W.C., 1932, Physiography and Glacial Geology of Eastern Montana and Adjacent Areas.

Alibrahim, M.A., 2016, Geological Mapping of Eastern Syria by using Remote sensing and GIS – characterization of the Euphrates water system: , p. 230.

Amundson, R., Heimsath, A., Owen, J., Yoo, K., and Dietrich, W.E., 2015, Hillslope soils and vegetation: Geomorphology, v. 234, p. 122–132, doi: 10.1016/j.geomorph.2014.12.031.

Appleby, P.G., and Oldfield, F., 1978, The calculation of lead-210 dates assuming a constant rate of supply of unsupported 210Pb to the sediment: Catena, v. 5, p. 1–8, doi: 10.1016/S0341-8162(78)80002-2.

Arno, S.F., and Habeck, J.R., 1972, Ecology of Alpine Larch (Larix lyallii Parl.) in the Pacific Northwest: v. 42, p. 417–450.

Belmont, P., Willenbring, J.K., Schottler, S.P., Marquard, J., Kumarasamy, K., and Hemmis, J.M., 2014, Toward generalizable sediment fingerprinting with tracers that are conservative and nonconservative over sediment routing timescales: Journal of Soils and Sediments, v. 14, p. 1479–1492, doi: 10.1007/s11368-014-0913-5.

Benjaram, S.S., 2017, Morphologic and Climatic Controls on Soil Evolution in the Bitterroot and Sapphire Mountains, Montana: , p. 150.

Bernhard, J.B.J., 1899, The Bitterroot forest reserve: Washington, p. 253-282.

Campbell, J.B., and Wynne, R.H., 2011, Introduction to Remote Sensing: New York, NY, The Guilford Press.

Chappell, A., Warren, A., Oliver, M.A., and Charlton, M., 1998, The utility of 137Cs for measuring soil redistribution rates in southwest Niger: Geoderma, v. 81, p. 313–337, doi: 10.1016/S0016-7061(97)00090-6.

Congalton, R.G., 1991, A review of assessing the accuracy of classifications of remotely sensed data: Remote Sensing of Environment, v. 37, p. 35–46, doi: 10.1016/0034-4257(91)90048-B.

Covington, W.W., Everett, R.L., Steele, R., Irwin, L.L., Daer, T.A., and Auclair, A.N.D., 1994, Historical and Anticipated Changes in Forest Ecosystems of the Inland West of the United States: Journal of Sustainable Forestry, v. 2, p. 13–62, doi: 10.1300/J091v02n01.

Dibiase, R.A., Heimsath, A.M., and Whipple, K.X., 2012, Hillslope response to tectonic forcing in threshold landscapes: Earth Surface Processes and Landforms, v. 37, p. 855–865, doi: 10.1002/esp.3205.

Dibiase, R.A., and Lamb, M.P., 2013, Vegetation and wildfire controls on sediment yield in bedrock landscapes: Geophysical Research Letters, v. 40, p. 1093–1097, doi: 10.1002/grl.50277.

Dietrich, W.E., and Perron, J.T., 2006, The search for a topographic signature of life.: Nature, v. 439, p. 411–418, doi: 10.1038/nature04452.

Dixon, J.L., and von Blanckenburg, F., 2012, Soils as pacemakers and limiters of global silicate weathering: Comptes Rendus - Geoscience, v. 344, p. 597–609, doi: 10.1016/j.crte.2012.10.012.

Dixon, J.L., and Riebe, C.S., 2014, Tracing and pacing soil across slopes: Elements, v. 10, p. 363–368, doi: 10.2113/gselements.10.5.363.

Dörr, H., 1995, Application of 210Pb in soils: Journal of Paleolimnology, v. 13, p. 157–168, doi: 10.1007/BF00678104.

Dorr, H., and Munnich, K., 1989, Downward movement of soil organic matter and its influence on trace element transport (210Pb, 137Cs) in the soil: Radiocarbon, v. 31, p. 655–663.

Dörr, H., and Münnich, K.O., 1991, Lead and cesium transport in european forest soils: Water, Air, and Soil Pollution, v. 57–58, p. 809–818, doi: 10.1007/BF00282944.

Faure, G., and Mensing, T.M., 2005, Isotopes: Principles and Applications.: Hoboken, NJ, USA, John Wiley & Sons, p. 928.

Gabet, E.J., 2003, Sediment transport by dry ravel: Journal of Geophysical Research: Solid Earth, v. 108, p. 1–8, doi: 10.1029/2001JB001686.

Gelfan, A.N., Pomeroy, J.W., and Kuchment, L.S., 2004, Modeling Forest Cover Influences on Snow Accumulation, Sublimation, and Melt: Journal of Hydrometeorology, v. 5, p. 785–803, doi: 10.1175/1525-7541.

Hahm, W.J., Riebe, C.S., Lukens, C.E., and Araki, S., 2014, Bedrock composition regulates mountain ecosystems and landscape evolution: Proceedings of the National Academy of Sciences, v. 111, p. 3338–3343, doi: 10.1073/pnas.1315667111.

He, Q., and Walling, D.E., 1996, Interpreting particle size effects in the adsorption of 137Cs and unsupported 210Pb by mineral soils and sediments: Journal of Environmental Radioactivity, v.30, p.117-137, doi:10.1016/0265-931X(96)89275-7.

He, Q., and Walling, D.E., 1997, The distribution of fallout 137Cs and 210Pb in undisturbed and cultivated soils: Applied Radiation and Isotopes, v. 48, p. 677–690, doi: 10.1016/S0969-8043(96)00302-8.

Heimsath, A.M., DiBiase, R.A., and Whipple, K.X., 2012, Soil production limits and the transition to bedrock-dominated landscapes: Nature Geoscience, v. 5, p. 210–214, doi: 10.1038/ngeo1380.

Heyerdahl, E.K., Brown, P.M., Kitchen, S.G., and Weber, M.H., 2011, Multicentury fire and forest histories at nineteen sites in Utah and eastern Nevada. Gen. Tech. Rep. RMRS-GTR-261WWW. Fort Collins, CO: U.S. Department of Agriculture, Forest Service, Rocky Mountain Research Station, p. 192.

Heyerdahl, E.K., Loehman, R.A., and Falk, D.A., 2014, Mixed-severity fire in lodgepole pine dominated forests: are historical regimes sustainable on Oregon's Pumice Plateau, USA? Canadian Journal of Forest Research, v. 44, p. 593–603, doi: 10.1139/cjfr-2013-0413.

Kaste, J.M., Heimsath, A.M., and Bostick, B.C., 2007, Short-term soil mixing quantified with fallout radionuclides: Geology, v. 35, p. 243–246, doi: 10.1130/G23355A.1.

Kaste, J.M., Heimsath, A.M., and Hohmann, M., 2006, Quantifying sediment transport across an undisturbed prairie landscape using cesium-137 and high resolution topography: Geomorphology, v. 76, p. 430–440, doi: 10.1016/j.geomorph.2005.12.007.

Kuz'min, P.P., 1960, Snow Accumulation and Methods of Estimating Snow Water Equivalents (in Russian): Hydrometeoizdat, p. 171.

Larsen, I.J., Almond, P.C., Eger, A., Stone, J.O., Montgomery, D.R., and Malcolm, B., 2014, Rapid Soil Production and Weathering in the Southern Alps, New Zealand: v. 343, p. 637–640.

Lewis, D.M., 1977, The use of 210Pb as a heavy metal tracer in the Susquehanna River system: Geochimica et Cosmochimica Acta, v. 41, p. 1557–1564, doi: 10.1016/0016-7037(77)90167-3.

Lonn, J.D., and Berg, R.B., 1996, Preliminary geologic map of the Bitterroot Valley, Montana: Montana Bureau of Mines Open-File Report 340, scale 1:100,000.

Lowdermilk, W.C., 1930, Influence of forest litter on run-off, percolation, and erosion.: Journal of Forestry, v. 28, p. 474–491.

Mabit, L., Meusburger, K., Fulajtar, E., and Alewell, C., 2013, The usefulness of 137Cs as a tracer for soil erosion assessment: A critical reply to Parsons and Foster (2011): Earth-Science Reviews, v. 127, p. 300–307, doi: 10.1016/j.earscirev.2013.05.008.

Marston, R.A., 2010, Geomorphology and vegetation on hillslopes: Interactions, dependencies, and feedback loops: Geomorphology, v. 116, p. 206–217, doi: 10.1016/j.geomorph.2009.09.028.

McWethy, D.B., Gray, Stephen, T., Higuera, P.E., Littell, J.S., Pederson, G.T., Ray, A.J., and Whitlock, C., 2010, Climate and Terrestrial Ecosystem Change in the U.S. Rocky Mountains and Upper Columbia Basin, p. 79.

Milodowski, D.T., Mudd, S.M., and Mitchard, E.T.A., 2015a, Erosion rates as a potential bottom-up control of forest structural characteristics in the Sierra Nevada Mountains: Ecology, v. 96, p. 31–38, doi: 10.1890/14-0649.1.

Milodowski, D.T., Mudd, S.M., and Mitchard, E.T.A., 2015b, Topographic roughness as a signature of the emergence of bedrock in eroding landscapes: Earth Surface Dynamics, v. 3, p. 483–499, doi: 10.5194/esurf-3-483-2015.

Miyata, S., Kosugi, K., Gomi, T., and Mizuyama, T., 2009, Effects of forest floor coverage on overland flow and soil erosion on hillslopes in Japanese cypress plantation forests: Water Resources Research, v. 45, p. 1–17, doi: 10.1029/2008WR007270.

Naylor, S., and Gabet, E.J., 2007, Valley asymmetry and glacial versus nonglacial erosion in the Bitterroot Range, Montana, USA: Geology, v. 35, p. 375–378, doi: 10.1130/G23283A.1.

Norton, K.P., von Blanckenburg, F., and Kubik, P.W., 2010, Cosmogenic nuclide-derived rates of diffusive and episodic erosion in the glacially sculpted upper rhone valley, Swiss Alps: Earth Surface Processes and Landforms, v. 35, p. 651–662, doi: 10.1002/esp.1961.

Norton, K.P., Molnar, P., and Schlunegger, F., 2014, Geomorphology The role of climate-driven chemical weathering on soil production: Geomorphology, v. 204, p. 510–517, doi: 10.1016/j.geomorph.2013.08.030.

Olofsson, P., Foody, G.M., Herold, M., Stehman, S. V., Woodcock, C.E., and Wulder, M.A., 2014, Good practices for estimating area and assessing accuracy of land change: Remote Sensing of Environment, v. 148, p. 42–57, doi: 10.1016/j.rse.2014.02.015.

Osaki, S., Tagawa, Y., Sugihara, S., Maeda, Y., and Inokura, Y., 2003, Transfer of 7Be, 210Pb and 210Po in a forest canopy of Japanese cedar: Journal of Radioanalytical and Nuclear Chemistry, v. 255, p. 449–454, doi: 10.1023/A:1022555626377.

Parsons, A.J., and Foster, I.D.L., 2011, What can we learn about soil erosion from the use of 137Cs? Earth-Science Reviews, v. 108, p. 101–113, doi: 10.1016/j.earscirev.2011.06.004.

Portenga, E.W., and Bierman, P.R., 2011, Understanding earth's eroding surface with 10Be: GSA Today, v. 21, p. 4–10, doi: 10.1130/G111A.1.

PRISM Climate Group No Title: Oregon State University, http://prism.oregonstate.edu (accessed February 2018).

Robichaud, P.R., Wagenbrenner, J.W., and Brown, R.E., 2010, Rill erosion in natural and disturbed forests: 1. Measurements: Water Resources Research, v. 46, p. 1–14, doi: 10.1029/2009WR008314.

Robichaud, P.R., Wagenbrenner, J.W., Brown, R.E., and Spigel, K.M., 2009, Three years of hillslope sediment yields following the valley complex fires Western Montana: USDA Forest Service - Research Paper RMRS-RP, p. 1–9.

Roering, J.J., Marshall, J., Booth, A.M., Mort, M., and Jin, Q., 2010, Evidence for biotic controls on topography and soil production: Earth and Planetary Science Letters, v. 298, p. 183–190, doi: 10.1016/j.epsl.2010.07.040.

Rogowski, A.S., and Tamura, T., 1970, Environmental mobility of cesium-137: Radiation Botany, v. 10, p. 35–45, doi: 10.1016/S0033-7560(70)80050-3.

Sankey, J.B., Kreitler, J., Hawbaker, T.J., McVay, J.L., Miller, M.E., Mueller, E.R., Vaillant, N.M., Lowe, S.E., and Sankey, T.T., 2017, Climate, wildfire, and erosion ensemble foretells more sediment in western USA watersheds: Geophysical Research Letters, v. 44, p. 8884–8892, doi: 10.1002/2017GL073979.

Stauffer, J.M., 1976, Ecology and floristics of Ohio Slide and other avalanche tracks in Lost Horse Canyon Bitterroot Mountains, Montana: University of Montana, p. 155.

Teramage, M.T., Onda, Y., Wakiyama, Y., Kato, H., Kanda, T., and Tamura, K., 2014, Environmental Science: Environmental Science: Processes & Impacts, v. 17, p. 110–119, doi: 10.1039/C4EM00402G.

USDA Farm Service Agency, 2015, National Agriculture Imagery Program, m_4611453_se_11_1_ 20151006_20160104.

Wainwright, J., Parsons, A.J., and Abrahams, A.D., 2000, Plot-scale studies of vegetation, overland flow and erosion interactions: Case studies from Arizona and New Mexico: Hydrological Processes, v. 14, p. 2921–2943, doi: 10.1002/1099-1085(200011/12)14:16/17<2921::AID-HYP127>3.0.CO;2-7.

Wakiyama, Y., Onda, Y., Mizugaki, S., Asai, H., and Hiramatsu, S., 2010, Soil erosion rates on forested mountain hillslopes estimated using 137Cs and 210Pbex: Geoderma, v. 159, p. 39–52, doi: 10.1016/j.geoderma.2010.06.012.

Walling, D.E., Collins, A.L., and Sichingabula, H.M., 2003, Using unsupported lead-210 measurements to investigate soil erosion and sediment delivery in a small Zambian catchment: Geomorphology, v. 52, p. 193–213, doi: 10.1016/S0169-555X(02)00244-1.

Walling, D.E., He, Q., and Quine, T.A., 1995, Use of caesium-137 and lead-210 as tracers in soil erosion investigations: IAHS-AISH, p. 163–172.

Whitlock, C., Shafer, S.L., and Marlon, J., 2003, The role of climate and vegetation change in shaping past and future fire regimes in the northwestern US and the implications for ecosystem management: Forest Ecology and Management, v. 178, p. 5–21, doi: 10.1016/S0378-1127(03)00051-3.

Wright, S.M., Howard, B.J., Strand, P., Nylén, T., and Sickel, M.A.K., 1999, Prediction of 137Cs deposition from atmospheric nuclear weapons tests within the Arctic: Environmental Pollution, v. 104, p. 131–143, doi: 10.1016/S0269-7491(98)00140-7.

Xiong, Y., Zeng, H., Xia, H., and Guo, D., 2014, Interactions between leaf litter and soil organic matter on carbon and nitrogen mineralization in six forest litter-soil systems: Plant and Soil, v. 379, p. 217–229, doi: 10.1007/s11104-014-2033-9.

Yang, H., and Appleby, P.G., 2016, Use of lead-210 as a novel tracer for lead (Pb) sources in plants: Scientific Reports, v. 6, p. 1–9, doi: 10.1038/srep21707.

Zapata, F., 2012, Handbook for the Assessment of Soil Erosion and Sedimentation Using Environmental Radionuclides: v. XXXIII, p. 81-87, doi: 10.1007/s13398-014-0173-7.2.

APPENDICES

APPENDIX A

FALLOUT RADIONUCLIDE RESULTS

Expanding on sample preparation and FRN analyses described in the Methods and Approach section, FRN samples were loaded into Canberra Industries high purity, broad energy germanium detectors (BEGe) to record ^{210}Pb (46.4 keV), ^{226}Ra (186 keV), ^{234Th} (63 keV), ^{235}U (186 keV), and ^{137}Cs (661 keV). Each isotope has a unique emission probability ^{210}Pb (4.18%), ^{226}Ra (3.5%), ^{234}Th (3.7%), ^{235}U (57.1%), and ^{137}Cs (85%) used with detector efficiency at each keV level: ^{210}Pb (12.23% and 12.8%), ^{226}Ra + ^{235}U (11.19% and 11.62%), ^{234}Th (14.31% and 14.96%), and ^{137}Cs (3.2% and 3.76%) for each detector, respectively. Samples were run for 24-48 hours to achieve a statistical count population (>500 counts/nuclide of interest) to ensure highest confidence in activities (counts/second/kilogram). CPS activities were then multiplied by the ratio of emission probability and respective detector efficiency to arrive at Becquerels/kg activities. We then went through Equations 1 and 2 to arrive at component and total site Inventories (Bq/m^2).

Table A1: FRN mineral and litter layer component activities

	Activity [Bq/kg]											
	Litter Layer (>2mm)			Litter Layer (<2mm)			Mineral Soil (>2mm)			Mineral Soil (<2mm)		
ID	^{210}Pb	$^{210}Pb_{ex}$	^{137}Cs	^{210}Pb	$^{210}Pb_{ex}$	^{137}Cs	^{210}Pb	$^{210}Pb_{ex}$	^{137}Cs	^{210}Pb	$^{210}Pb_{ex}$	^{137}Cs
F1	291.3	291.3	33.6	472.1	472.1	66.9	160.7	144.8	36.2	131.7	118.2	62.5
F2	346.9	346.9	73.4	373.0	351.2	106.1	56.3	56.3	16.3	67.7	47.7	26.6
F3	153.5	153.5	27.2	194.8	194.8	41.3	17.0	1.8	2.5	20.3	3.8	5.6
F4	162.2	162.2	22.9	433.3	433.3	120.7				35.7	12.8	17.2
F5	496.6	496.6	44.1	565.9	565.9	101.2	177.0	129.8	66.5	98.3	80.1	39.5
F6	466.8	460.6	76.0	527.2	511.6	103.2	1.6	0.0	9.0	65.1	47.5	18.5
F7	178.2	178.2	11.4	389.3	389.3	38.3	7.6	0.7	0.4	17.8	3.1	5.6
F8	398.3	398.3	22.8	716.5	716.5	97.6	12.4	2.1	2.4	59.0	44.8	26.2
F9	599.3	599.3	63.0	952.9	952.9	232.0	10.2	2.8	1.1	49.7	29.2	12.6
F10	389.0	375.2	46.7	545.7	545.7	91.0	18.8	11.7	3.0	20.1	6.0	7.6
F11	461.6	461.6	103.7	556.0	556.0	111.7	117.1	117.1	29.1	164.8	145.3	66.2
F12	744.2	744.2	73.5	855.5	855.5	211.8	13.0	3.9	0.8	23.6	4.5	8.2
F13	285.8	285.8	34.8	496.6	496.6	89.0	16.0	8.9	3.5	76.2	54.7	23.9
F14	825.0	825.0	40.8	919.2	909.2	168.0	28.0	28.0	8.3	64.3	43.6	33.7
F15	215.0	215.0	151.8	758.3	758.3	217.3	30.1	30.1	12.0	70.7	51.0	32.6
F16	852.0	852.0	55.3	821.2	821.2	80.8	25.1	13.7	5.6	75.4	58.7	20.4
F17	520.5	520.5	30.2	667.9	629.4	109.4	9.2	2.8	0.4	21.1	6.9	6.2
NF1							84.0	84.0	27.7	117.6	97.0	27.2
NF2							13.5	0.9	2.8	61.0	53.4	12.2
NF3							31.6	16.5	6.4	64.5	34.3	15.4
NF4							60.7	44.0	14.3	74.7	48.2	23.4
NF5							22.1	9.0	7.2	92.5	62.2	29.3
NF6							14.1	2.1	4.1	62.5	32.3	20.8
NF7							14.0	4.4	4.2	93.7	70.8	25.5
NF8							10.8	1.0	2.6	59.2	39.1	17.5
NF9							14.2	5.8	4.8	78.3	58.4	27.4
NF10							57.0	43.5	12.6	92.0	74.7	33.0
NF11							170.8	157.1	61.7	194.7	178.4	67.7
NF12							71.5	71.5	7.8	109.5	91.4	23.0
NF13							15.1	9.2	5.5	94.2	74.0	37.7
NF14							98.0	89.8	18.4	262.9	237.7	66.8
NF15							23.7	12.5	6.7	137.7	118.8	48.6
NF16							355.1	355.1	28.8	224.0	196.7	82.2
NF17							72.9	72.9	16.6	213.7	193.8	68.4
NF18							67.5	67.5	10.2	229.3	207.0	77.7
NF19							11.0	0.3	3.0	92.9	76.8	33.3

Table A2: FRN mineral and litter layer component inventories

	Inventory [Bq/m2]											
	Litter Layer (>2mm)			Litter Layer (<2mm)			Mineral Soil (>2mm)			Mineral Soil (<2mm)		
ID	^{210}Pb	$^{210}Pb_{ex}$	^{137}Cs	^{210}Pb	$^{210}Pb_{ex}$	^{137}Cs	^{210}Pb	$^{210}Pb_{ex}$	^{137}Cs	^{210}Pb	$^{210}Pb_{ex}$	^{137}Cs
F1	4.32	4.32	0.50	4.80	4.80	0.68	13.16	11.81	6.25	8.41	7.57	1.89
F2	6.35	6.35	1.34	7.16	6.74	2.04	4.86	3.43	1.91	2.85	2.85	0.83
F3	1.02	1.02	0.18	1.63	1.63	0.34	3.13	0.59	0.87	1.42	0.15	0.21
F4	0.00	0.00	0.00	2.84	2.84	0.79	3.20	1.14	1.54	0.00	0.00	0.00
F5	7.65	7.65	0.68	5.43	5.43	0.97	3.64	2.97	1.46	3.97	2.91	1.49
F6	7.19	7.09	1.17	5.06	4.91	0.99	6.65	4.85	1.89	0.08	0.00	0.43
F7	2.18	2.18	0.14	4.98	4.98	0.49	1.70	0.30	0.53	0.84	0.08	0.05
F8	2.43	2.43	0.14	2.80	2.80	0.38	6.52	4.95	2.89	0.86	0.15	0.16
F9	7.29	7.29	0.77	12.23	12.23	2.98	3.50	2.06	0.89	0.71	0.19	0.07
F10	9.65	9.31	1.16	8.29	8.29	1.38	0.89	0.27	0.34	0.38	0.24	0.06
F11	9.42	9.42	2.12	10.89	10.89	2.19	2.26	2.00	0.91	0.65	0.65	0.16
F12	6.29	6.29	0.62	14.16	14.16	3.51	2.60	0.50	0.91	0.34	0.10	0.02
F13	1.29	1.29	0.16	5.21	5.21	0.93	4.02	2.88	1.26	0.33	0.18	0.07
F14	2.44	2.44	0.12	1.88	1.86	0.34	4.83	3.28	2.54	0.98	0.98	0.29
F15	0.98	0.98	0.69	4.11	4.11	1.18	8.43	6.09	3.89	1.10	1.10	0.44
F16	15.97	15.97	1.04	5.13	5.13	0.51	5.13	3.99	1.38	1.33	0.72	0.29
F17	0.53	0.53	0.03	0.99	0.94	0.16	3.31	1.08	0.97	0.64	0.20	0.03
NF1							13.09	10.80	3.02	5.35	5.35	1.77
NF2							6.88	6.03	1.38	1.36	0.09	0.28
NF3							9.13	4.86	2.18	1.94	1.01	0.39
NF4							9.10	5.88	2.85	3.44	2.49	0.81
NF5							11.64	7.83	3.68	2.37	0.96	0.77
NF6							11.13	5.75	3.70	1.26	0.18	0.36
NF7							10.37	7.84	2.83	0.68	0.21	0.20
NF8							9.99	6.60	2.96	0.84	0.08	0.20
NF9							10.00	7.46	3.50	1.41	0.58	0.48
NF10							10.91	8.86	3.91	6.60	5.05	1.46
NF11							10.18	9.32	3.54	9.31	8.56	3.36
NF12							10.43	8.71	2.19	4.20	4.20	0.46
NF13							13.75	10.80	5.50	1.37	0.84	0.50
NF14							11.64	10.53	2.96	1.97	1.81	0.37
NF15							9.46	8.16	3.34	0.57	0.30	0.16
NF16							21.35	18.75	7.83	10.90	10.90	0.88
NF17							10.31	9.35	3.30	1.59	1.59	0.36
NF18							19.56	17.66	6.63	1.92	1.92	0.29
NF19							7.82	6.47	2.80	0.88	0.02	0.24

Table A3: FRN total site activities and inventories

	Total Site Activities (Bq/kg)			<2mm Total Site Inventories (Bq/m2)			Total Site Inventories (Bq/m2)		
ID	**^{210}Pb**	**$^{210}Pb_{ex}$**	**^{137}Cs**	**^{210}Pb**	**$^{210}Pb_{ex}$**	**^{137}Cs**	**^{210}Pb**	**$^{210}Pb_{ex}$**	**^{137}Cs**
F1	567.90	553.53	132.36	17.96	16.61	6.93	30.69	28.50	9.32
F2	478.87	433.54	134.45	12.02	10.17	3.95	21.22	19.37	6.12
F3	221.67	194.55	49.21	4.76	2.22	1.21	7.20	3.39	1.60
F4	307.9*	292.7*	90.5*	6.04	3.99	2.33	ND	ND	ND
F5	685.01	646.75	131.77	9.07	8.40	2.44	20.69	18.96	4.61
F6	543.18	512.38	103.83	11.71	9.76	2.88	18.97	16.85	4.48
F7	326.69	301.64	33.68	6.68	5.28	1.02	9.70	7.53	1.21
F8	622.31	584.69	88.04	9.32	7.75	3.27	12.61	10.33	3.58
F9	878.57	837.95	180.33	15.73	14.29	3.87	23.73	21.77	4.71
F10	494.50	452.76	81.36	9.19	8.56	1.72	19.21	18.10	2.94
F11	710.80	669.26	177.61	13.16	12.89	3.10	23.22	22.96	5.37
F12	856.30	822.28	175.68	16.76	14.66	4.41	23.39	21.05	5.06
F13	556.22	519.88	106.30	9.24	8.10	2.19	10.85	9.57	2.42
F14	937.30	898.08	122.36	6.71	5.14	2.88	10.13	8.56	3.29
F15	585.44	561.73	220.39	12.54	10.20	5.07	14.62	12.28	6.20
F16	1005.64	960.97	90.56	10.26	9.13	1.89	27.56	25.82	3.22
F17	673.78	615.98	90.53	4.31	2.02	1.13	5.48	2.74	1.19
NF1	232.24	213.14	61.93	13.09	10.80	3.02	18.44	16.15	4.79
NF2	141.95	116.56	52.62	6.88	6.03	1.38	8.24	6.13	1.66
NF3	125.60	60.40	25.98	9.13	4.86	2.18	11.07	5.87	2.57
NF4	124.53	79.00	40.47	9.10	5.88	2.85	12.54	8.37	3.66
NF5	158.61	126.22	40.23	11.64	7.83	3.68	14.01	8.79	4.45
NF6	160.51	66.79	55.10	11.13	5.75	3.70	12.39	5.93	4.06
NF7	129.78	95.28	37.54	10.37	7.84	2.83	11.05	8.05	3.03
NF8	81.06	38.24	33.38	9.99	6.60	2.96	10.83	6.67	3.16
NF9	80.37	49.84	27.71	10.00	7.46	3.50	11.42	8.04	3.99
NF10	145.42	107.39	50.40	10.91	8.86	3.91	17.51	13.91	5.38
NF11	244.95	209.98	96.34	10.18	9.32	3.54	19.48	17.88	6.90
NF12	274.31	235.36	52.56	10.43	8.71	2.19	14.63	12.91	2.64
NF13	109.69	94.96	38.66	13.75	10.80	5.50	15.11	11.63	6.00
NF14	467.74	430.94	116.30	11.64	10.53	2.96	13.61	12.34	3.33
NF15	168.94	140.39	52.12	9.46	8.16	3.34	10.03	8.46	3.50
NF16	378.03	337.56	106.08	21.35	18.75	7.83	32.24	29.65	8.71
NF17	237.33	210.55	69.00	10.31	9.35	3.30	11.89	10.94	3.66
NF18	312.49	261.89	99.58	19.56	17.66	6.63	21.48	19.58	6.92
NF19	106.67	71.00	43.02	7.82	6.47	2.80	8.71	6.49	3.05

APPENDIX B

SPATIAL DATA ASSESSMENT

Simplified Spatial Processing Workflow

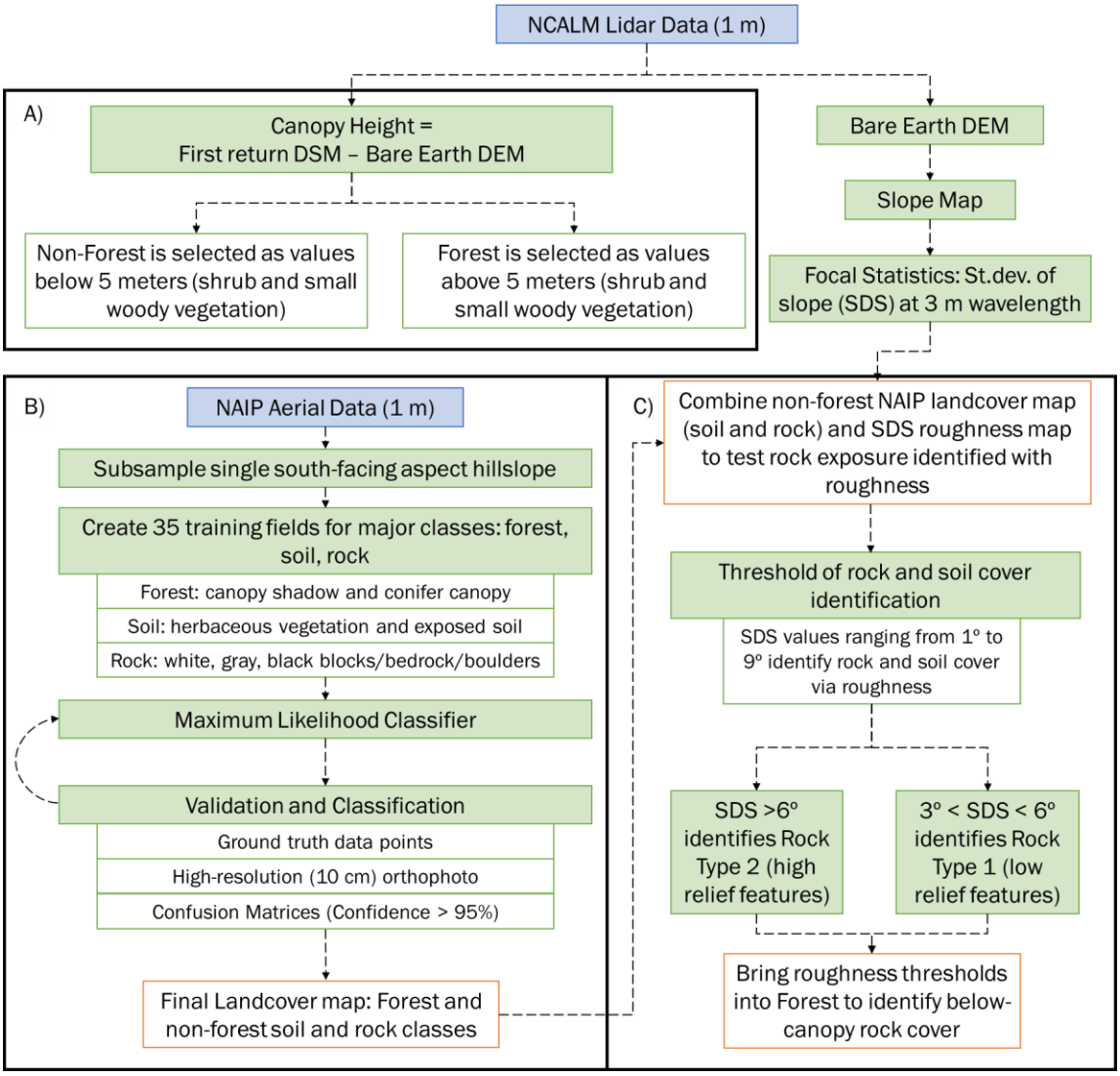

Figure A1. Flowchart of geospatial methods. Panel A shows GIS methods used in the field to inform sample collection in forested and non-forested regions. Panel B shows remote sensing methods that lead to a 1m spatial resolution landcover map of soil, rock, and forest cover. Panel C combines these pathways to first identify non-forest rock roughness and then below-canopy rock distribution.

Accuracy Assessment: Confusion Matrices

Confusion or error matrices were formed by using the original NAIP image region based on high-resolution aerial orthophotos (15cm pixels) and ground reference data. We assigned 40 pixels for soil, forest, and rock (41) each and 16 pixels for water, due to low number of pixels (Campbell and Wynne, 2011; Congalton, 1991; Olofsson et al., 2014). These pixels were assigned to border areas near neighboring classes and thus will under-predict overall map accuracy by highlighting pixels most likely to by misclassified (i.e., border pixels). The manually classified pixels were then compared to NAIP landcover classified maps to validate accuracy using the confusion matrix (Table A4). We use overall accuracy to assess the level of pixel assignment accuracy for the classified maps calculated as the sum of diagonal cells in Table A4 divided by n. Table A5 is the final produced NAIP map. The finalized NAIP map contained four landcover classes where n represents the number of pixels in each class (m^2): rock (n = 10,031), water (n = 944), soil (n = 8,597), and forest (n = 13,846).

		Reference Points				
		Rock	Water	Soil	Forest	Total
NAIP map	Rock	p_{11}	p_{12}	p_{13}	p_{14}	p_{1-}
	Water	p_{21}	p_{22}	p_{23}	p_{24}	p_{2-}
	Soil	p_{31}	p_{32}	p_{33}	p_{34}	p_{3-}
	Forest	p_{41}	p_{41}	p_{41}	p_{41}	p_{4-}
	Total	p_{-1}	p_{-2}	p_{-3}	p_{-4}	n

Table A4: Confusion or error matrix adapted from Olofsson et al. 2014. Here p represents the count of pixels in each respective class by class relationship and n is the total number of reference points. Counts that occur in the diagonal are considered to agree between datasets.

		Reference Points				
		Rock	Water	Soil	Forest	Total
NAIP map	Rock	*41*	5	1	0	47
	Water	0	*10*	0	0	10
	Soil	0	0	*36*	4	40
	Forest	0	1	3	*36*	40
	Total	41	16	40	40	135

Table A5: Data from finalized majority filter NAIP classified landcover map yields an overall accuracy of 97.1%.

APPENDIX C

FIELD OBSERVATIONS AND FINDINGS

Table A6: Forested soil thicknesses [meters] where DUFF is the litter layer

	Soil Grid Depths								Thickness		
Sample	**1**	**2**	**3**	**4**	**5**	**6**	**7**	**8**	**Average**	**Auger**	**Litter**
F1	0.15	0.2	0.12	0.1	0.2	0.2	0.2	0.02	0.16	0.2	0.05
F1AUG1										0.2	
F1DUFF											0.075
F2	0.2	0.2	0.18	0.07	0.2	0.2	0.2	0.05	0.16	0.25	0.075
F2AUG1										0.2	
F2AUG2										0.05	
F2DUFF											0.075
F3	0.2	0.2	0.2	0.2	0.2	0.2	0.2	0.15	0.19	0.2	0.03
F3AUG1										0.2	
F3DUFF											0.03
F4	0.2	0.03	0.01	0.2	0.2	0.12	0.07	0.1	0.12	0.2	0.02
F4AUG1										0.2	
F4DUFF											0.02
F5	0.04	0.18	0.2	0.02	0	0.1	0.02	0.18	0.09	0.19	0.05
F5AUG1										0.19	
F5DUFF											0.05
F6	0.02	0.07	0.2	0.2	0.2	0.17	0.2	0.2	0.16	0.4	0.05
F6AUG1										0.2	
F6AUG2										0.2	
F6DUFF											0.05
F7	0.2	0.2	0.2	0.18	0.2	0.2	0.2	0.2	0.20	0.3	0.05
F7AUG1										0.2	0.05
F7AUG2										0.1	
F7DUFF											0.05
F8	0.07	0.2	0.2	0.1	0.2	0.04	0.2	0.18	0.15	0.35	0.02
F8AUG1										0.2	0.02
F8AUG2										0.15	
F8DUFF											0.02
F9	0.2	0.2	0	0.2	0	0.2	0.2	0.2	0.15	0.52	0.05
F9AUG1										0.2	0.05
F9AUG2										0.2	
F9AUG3										0.12	
F9DUFF											0.05
F10	0.18	0.14	0	0.2	0.1	0.2	0.09	0.1	0.13	0.4	0.08
F10AUG1										0.2	0.08
F10AUG2										0.2	
F10DUFF											0.08
F11	0	0.08	0.12	0	0.05	0.16	0.19	0.15	0.09	0.3	0.08
F11AUG1										0.2	0
F11AUG2										0.4	0
F11DUFF											0.08
F12	0.2	0.1	0.2	0.05	0.03	0.2	0.2	0.2	0.15	0.33	0.05
F12AUG1										0.2	

F12AUG2										0.13	
F12DUFF											0.05
F13	0.17	0.05	0.01	0.01	0.14	0.03	0.2	0.05	0.08	0.27	0.03
F13AUG1										0.2	
F13AUG2										0.07	
F13DUFF											0.03
F14	0.18	0.06	0.08	0.15	0.01	0.02	0.07	0.14	0.09	0.38	0.01
F14AUG1										0.2	
F14AUG2										0.18	
F14DUFF											0.01
F15	0.12	0	0.02	0.09	0.35	0.07	0.2	0.2	0.13	0.2	0.02
F15AUG1										0.2	
F15DUFF											0.02
F16	0.2	0.05	0.07	0.15	0.2	0.18	0.2	0.04	0.14	0.6	0.05
F15AUG1										0.2	
F16AUG2										0.2	
F16AUG3										0.2	
F16DUFF											0.05
F17	0.2	0.2	0.2	0.15	0.15	0.18	0.1	0.16	0.17	0.35	0.005
F17AUG1										0.2	
F17AUG2										0.15	
F17DUFF											0.005

Table A7: Non-forested soil thicknesses [meters]

	Soil Grid Depths								Thickness	
Sample	**1**	**2**	**3**	**4**	**5**	**6**	**7**	**8**	**Average**	**Auger**
NF1	0.1	0.2	0.15	0.2	0.07	0.02	0.1	0.16	0.13	0.15
NF1AUG1										0.15
NF2	0.18	0.02	0.18	0.17	0.2	0.2	0.2	0.07	0.15	0.2
NF2AUG1										0.2
NF3	0.03	0.19	0.09	0.2	0.18	0.2	0.12	0.15	0.15	0.3
NF3AUG1										0.2
NF3AUG2										0.1
NF4	0.15	0.07	0.05	0.15	0.12	0.2	0.1	0.18	0.13	0.1
NF4AUG1										0.1
NF5	0.1	0.2	0.2	0.2	0.08	0.2	0.15	0.2	0.17	0.15
NF5AUG1										0.15
NF6	0.2	0.15	0.2	0.18	0.2	0.2	0.2	0.2	0.19	0.75
NF6AUG1										0.2
NF6AUG2										0.2
NF6AUG3										0.2
NF6AUG4										0.15
NF7	0.2	0.2	0.15	0.02	0.02	0.1	0.12	0.1	0.11	0.19
NF7AUG1										0.19
NF8	0.2	0.2	0.15	0.2	0.15	0.2	0.11	0.2	0.18	0.5
NF8AUG1										0.2
NF8AUG2										0.2
NF8AUG3										0.1
NF9	0.2	0.04	0.2	0.14	0.2	0.2	0.2	0.12	0.16	0.17
NF9AUG1										0.17
NF10	0.1	0.18	0.2	0.2	0.18	0.16	0.2	0.12	0.17	0.1
NF10AUG1										0.1
NF11	0	0.02	0.12	0.06	0.08	0.1	0.03	0.2	0.08	0.25
NF11AUG1										0.2
NF11AUG2										0.05
NF12	0.2	0.2	0.05	0.1	0.08	0.12	0.06	0.07	0.11	0.27
NF12AUG1										0.2
NF12AUG2										0.07
NF13	0.05	0.05	0.02	0.13	0.18	0.07	0.15	0.7	0.17	0.16
NF13AUG1										0.16
NF14	0.06	0.04	0.12	0.06	0.02	0.15	0.12	0.05	0.08	0.05
NF14AUG1										0.05
NF15	0.1	0.04	0.05	0.07	0.05	0.04	0.08	0.1	0.07	0.12
NF15AUG1										0.12
NF16	0.09	0.03	0.14	0.12	0.1	0	0.19	0.05	0.09	0.2
NF16AUG1										0.2
NF17	0.07	0.16	0.05	0.02	0	0.03	0.02	0.05	0.05	0.19
NF17AUG1										0.19
NF18	0.02	0.03	0.04	0.07	0.05	0.18	0.17	0.09	0.08	0.27

NF18AUG1										0.2
NF18AUG2										0.07
NF19	0.12	0.05	0.1	0.2	0.2	0.2	0.07	0	0.12	0.32
NF19AUG1										0.2
NF19AUG2										0.12

Table A8: Forested soil cover

Sample	Soil Cover 1	2	3	4	5	6	7	8	Auger Soil Cover	Average Soil Cover
F1	1	0.95	1	1	1	0.8	0.95	0.67	1	93%
F1AUG1										
F1DUFF										
F2	1	1	1	1	1	1	0.6	1	1	96%
F2AUG1									1	100%
F2AUG2									1	100%
F2DUFF										
F3	1	1	1	1	1	1	1	1	1	100%
F3AUG1									1	100%
F3DUFF										
F4	0.9	0.9	0.55	0.4	1	0.85	0.9	0.8	0.9	80%
F4AUG1									0.9	90%
F4DUFF										
F5	1	1	1	0.3	0	0.2	0.33	1	0.9	64%
F5AUG1									0.9	90%
F5DUFF										
F6	1	1	1	1	1	0.75	0.75	0.88	1	93%
F6AUG1									1	100%
F6AUG2									1	100%
F6DUFF										
F7	1	1	1	1	1	1	1	1	1	100%
F7AUG1									1	100%
F7AUG2									1	100%
F7DUFF										
F8	1	1	1	0.875	1	0.5	1	1	1	93%
F8AUG1									1	100%
F8AUG2									1	100%
F8DUFF										
F9	1	1	1	1	1	1	1	1	1	100%
F9AUG1									1	100%
F9AUG2									1	100%
F9AUG3									1	100%
F9DUFF										
F10	1	1	1	1	1	1	1	1	1	100%
F10AUG1									1	100%
F10AUG2									1	100%
F10DUFF										
F11	0	1	0.85	1	0.75	1	1	1	1	84%
F11AUG1									1	100%
F11AUG2										
F11DUFF										

F12	1	1	1	1	1	1	1	1	1	100%
F12AUG1									1	100%
F12AUG2									1	100%
F12DUFF										
F13	0.9	1	1	0.5	1	1	1	1	1	93%
F13AUG1									1	100%
F13AUG2									1	100%
F13DUFF										
F14	1	1	1	1	1	1	1	1	1	100%
F14AUG1									1	100%
F14AUG2									1	100%
F14DUFF										
F15	0.5	0	0.5	1	1	0.9	0.6	1	0.9	71%
F15AUG1									0.9	90%
F15DUFF										
F16	0.6	0.9	1	1	1	1	1	1	1	94%
F15AUG1									1	100%
F16AUG2									1	100%
F16AUG3									1	100%
F16DUFF										
F17	1	1	0.9	1	1	1	1	1	1	99%
F17AUG1									1	100%
F17AUG2									1	100%
F17DUFF										

Table A9: Non-forested soil cover

Sample	Soil Cover 1	2	3	4	5	6	7	8	Auger Soil Cover	Average Soil Cover
NF1	0.4	0.88	0.95	1	0.8	0.85	1	1	1	88%
NF1AUG1									1	100%
NF2	0.95	0.4	0.95	0.95	1	0.95	0.9	1	0.9	89%
NF2AUG1									0.9	90%
NF3	0.1	1	1	1	1	1	1	1	1	90%
NF3AUG1									1	100%
NF3AUG2									1	100%
NF4	0.1	1	1	1	1	1	0.95	0.9	1	88%
NF4AUG1									1	100%
NF5	1	0.95	1	1	1	1	1	1	1	99%
NF5AUG1									1	100%
NF6	1	0.85	0.5	1	1	1	1	1	1	93%
NF6AUG1									1	100%
NF6AUG2									1	100%
NF6AUG3									1	100%
NF6AUG4									1	100%
NF7	1	1	0.67	0.95	0.4	0.7	1	1	0.62	82%
NF7AUG1									0.62	62%
NF8	1	1	0.8	0.88	0.88	1	1	1	1	95%
NF8AUG1									1	100%
NF8AUG2									1	100%
NF8AUG3									1	100%
NF9	1	1	1	1	1	1	1	0.95	1	99%
NF9AUG1									1	100%
NF10	1	1	1	1	1	1	1	1	1	100%
NF10AUG1									1	100%
NF11	0	0.75	1	1	1	1	1	0.6	1	82%
NF11AUG1									1	100%
NF11AUG2									1	100%
NF12	1	0.7	1	0.75	0.75	0.85	0.8	1	0.85	86%
NF12AUG1									0.85	85%
NF12AUG2									0.85	85%
NF13	0.6	1	1	0.8	1	1	0.2	0.4	1	78%
NF13AUG1									1	100%
NF14	0.6	0.8	0.6	0.6	0.75	0.4	0.95	0.7	0.7	68%
NF14AUG1									0.7	70%
NF15	1	0.88	0.75	0.875	0.875	1	1	1	0.75	90%
NF15AUG1									0.75	75%
NF16	1	1	1	1	1	0	0.7	1	1	86%
NF16AUG1									1	100%
NF17	1	1	1	0.75	0	0.1	0.8	0.7	1	71%

NF17AUG1									1	100%
NF18	1	1	1	0.8	1	0.75	1	0.8	1	93%
NF18AUG1									1	100%
NF18AUG2									1	100%
NF19	1	0.8	0.8	1	1	1	1	0	1	84%
NF19AUG1									1	100%
NF19AUG2									1	100%